Dual role of Miro protein clusters in mitochondrial cristae organisation and ER-Mitochondria Contact Sites

Souvik Modi[1,6#], Guillermo López-Doménech[1#], Elise F. Halff[1,7], Christian Covill-Cooke[1], Davor Ivankovic[1], Daniela Melandri[1], Lorena Arancibia-Cárcamo[1], Jemima J. Burden[5], Alan R. Lowe[2,3,4], Josef T. Kittler[1]

[#] These authors contributed equally.

[1]Neuroscience, Physiology and Pharmacology, University College London, Gower Street, WC1E 6BT, London, UK.

[2]Structural & Molecular Biology, University College London, Gower Street, WC1E 6BT, London, UK.

[3]Department of Biological Sciences, Birkbeck College London, WC1E 7H, London, UK.

[4]London Centre for Nanotechnology, 17-19 Gordon Street, WC1H 0AH, London, UK.

[5]MRC Laboratory for Molecular Cell Biology, University College London, Gower Street, WC1E 6BT, London, UK.

[6]Department of Biological Sciences, Tata Institute of Fundamental Research, Homi Bhaba Road, Mumbai, 400005, India.

[7]Present address: Department of Psychosis studies, Institute of Psychiatry, Psychology and Neuroscience, King's College London, 16 De Crespigny Park, SE5 8AB, London, UK.

Corresponding Author

To whom correspondence should be addressed. E-mail: j.kittler@ucl.ac.uk.

Keywords: Rhot1, Rhot2, TRAK1, TRAK2, Mic19, CHCHD3, Mic60, Mitofilin, Sam50, MIB, dSTORM, SIM, BN-PAGE

Abstract

Mitochondrial Rho (Miro) GTPases localize to the outer mitochondrial membrane and are essential machinery for the regulated trafficking of mitochondria to defined subcellular locations. However, their sub-mitochondrial localization and relationship with other critical mitochondrial complexes remains poorly understood. Here, using super-resolution fluorescence microscopy, we report that Miro proteins form nanometer-sized clusters along the mitochondrial outer membrane in association with the Mitochondrial Contact Site and Cristae Organizing System (MICOS). Using knockout mouse embryonic fibroblasts (MEF) we show that Miro1 and Miro2 are required for normal mitochondrial cristae architecture and endoplasmic reticulum-mitochondria contacts sites (ERMCS). Further, we show that Miro couples MICOS to TRAK motor protein adaptors to ensure the concerted transport of the two mitochondrial membranes and the correct distribution of cristae on the mitochondrial membrane. The Miro nanoscale organization, association with MICOS complex and regulation of ERMCS reveal new levels of control of the Miro GTPases on mitochondrial functionality.

Introduction

Mitochondria are the powerhouse of cells, generating ATP to drive key cellular functions including ion pumping, intracellular trafficking and cellular signalling cascades[1-7]. The mitochondrial population are trafficked to where they are needed to meet local energy and Ca^{2+} buffering demands, by motor and adaptor proteins found on their outer surface that tether these organelles to the cytoskeleton[8-11]. Miro proteins form complexes with the TRAK adaptors and dynein/kinesin motors to regulate the microtubule-dependent transport of mitochondria[7,12]. Recently, an actin-dependent transport of mitochondria has also been linked to Miro regulation through the recruitment and stabilization of the mitochondrial myosin 19 (Myo19) to the outer mitochondrial membrane[13,14]. In yeast Miro exists as a single orthologue, Gem1, important for correct mitochondrial inheritance and cellular viability[15-17]. In mammals there are two Miro family members, Miro1 and Miro2, that share ~60% sequence identity, comprising two GTPase domains flanking two EF-hand Ca^{2+}-binding domains and a C-terminal transmembrane domain that targets them to the Outer Mitochondrial Membrane (OMM)[12,18]. Although their role in mitochondrial transport is well established, far less is known about their interactions with other key protein complexes located at the OMM or the Inner Mitochondrial Membrane (IMM).

The mitochondrial contact site and cristae organizing system (MICOS) located in the IMM, is a large protein complex (often >1 MDa) mainly formed by Mic60/Mitofilin, Mic19/CHCHD3, Mic10/MINOS1 and Mic25/CHCHD6[19-29]. Optical and electron microscopy, have revealed that constituents of the MICOS complex are concentrated in discrete patches on the IMM decorating the cristae junctions[30,31]. The MICOS complex is crucial for maintaining cristae architecture as knockdown of MICOS components leads to mitochondria with altered cristae morphology

resulting in compromised oxidative phosphorylation[28,32,33]. In addition, the MICOS complex acts as a bridge between the OMM and the IMM by forming a higher order complex with Sam50, known as the Mitochondria Intermembrane Bridging complex (MIB)[34,35]. Although it is postulated that the yeast homologue of mammalian Miro GTPases, Gem1, and *Drosophila* homologue, dMiro, could be associated with individual MICOS components[36,37], association of mammalian Miro proteins with intact MICOS complex and its functional role has not yet been characterized. Mitochondria also engage in physical interaction with the endoplasmic reticulum (ER) through dedicated protein complexes at contact sites, known as ERMES (ER-Mitochondria Encounter Structures) in yeast or ER-Mitochondria contact sites (ERMCS) in mammals[38-40]. Yeast Gem1 and *Drosophila* dMiro have been identified as integral parts of the ERMES and ERMCS complexes respectively[15,16,41,42]. Interaction mapping in yeast established that ERMES components and MICOS complex genes shared a strong genetic interaction between them and also identified similar interactions with *gem1*[36]. However, the relationship between Miro proteins and the MICOS and ERMCS complexes in mammalian cells remains largely unexplored.

By combining biochemical, super-resolution and electron microscopy techniques, we address here the roles of mammalian Miro proteins in the regulation of mitochondrial cristae architecture and ER-mitochondrial contact-sites in mammalian cells. Genetic ablation of both Miro proteins in mouse embryonic fibroblasts (MEF) results in reduced ERMCS and in the disruption of mitochondrial cristae organization. Using Structured Illumination Microscopy (SIM) and dual color direct Stochastic Optical Reconstruction Microscopy (dSTORM) imaging of mitochondria, we show the sub-mitochondrial organization of Miro proteins. Miro1 and Miro2 form discrete clusters on the mitochondrial membrane the distribution of which closely correlate with MICOS

components. Biochemically, we show that Miro1 and Miro2 form a protein complex with Sam50 and MICOS. Furthermore, we also show that Miro proteins link these MIB/MICOS complexes spanning the inner and outer mitochondrial membranes to the motor adaptor proteins TRAK1 and TRAK2. Our data establish a novel role for Miro proteins in connecting the mitochondrial transport machinery with the MICOS complexes to ensure the coordinated transport of both mitochondrial membranes and the homogeneous distribution of cristae and cristae junctions inside the mitochondria. Miro proteins, thus, guarantee the appropriate supply of the mitochondrial compartments responsible for energy production to the regions in the cell where mitochondria are delivered.

Results

Loss of Miro1 and Miro2 alters mitochondrial ultrastructure

We recently showed that loss of both Miro proteins in MEFs leads to altered mitochondrial distribution and morphology[13]. To further explore the effects of Miro loss on mitochondrial morphology and structure we performed Structured Illumination Microscopy (SIM), a super-resolution imaging procedure that provides an optical resolution almost twice the diffraction limit[43]. Using SIM, wild type (WT) cells expressing a mitochondrial matrix targeted GFP ($mtRo^{GFP}$) showed a predominance of thin and long mitochondria, with individual mitochondria having continuous GFP staining with occasional cells presenting short and round mitochondria (Fig. 1A and B). In contrast, about 70% of Miro1/2 double knockout (DKO) cells presented a discontinuous and often hollow matrix-targeted GFP signal (Fig. 1A and B) which correlated with a predominance of shorter mitochondria with enlarged and more rounded mitochondrial segments. The discontinuous mitochondrial matrix suggests a role for Miro proteins in maintaining the architecture of the inner mitochondrial membranes. Importantly, re-expression of either ^{Myc}Miro1 or ^{Myc}Miro2 in DKO cells rescued mitochondrial matrix continuity (Fig. 1B, Supplementary Fig. 1).

To further explore the effects of depleting Miro proteins on mitochondrial structure and morphology, we carried out ultrastructural analysis of MEF cells using Transmission Electron Microscopy (TEM). In WT MEFs, the majority of mitochondria showed normal cristae structure and a homogeneous cristae distribution throughout the mitochondrial segments (Fig. 1C, D and E). In contrast, the majority of DKO cells presented an altered cristae architecture with frequent vesiculated mitochondrial matrix (Fig. 1C and D). Importantly, DKO cells showed a non-uniform

arrangement of the mitochondrial cristae, with some mitochondrial regions having the normal density of cristae alternated with regions that appeared enlarged and devoid of cristae (Fig. 1E). Together, these data indicate that Miro proteins play a role in regulating mitochondrial morphology and in the maintenance of the internal structure of the mitochondrial membranes and mitochondrial cristae architecture.

To test whether these changes in mitochondrial structure could be a consequence of reduced levels of protein components known to regulate cristae structure we carried out western blot analysis of lysates from three different WT and DKO MEF lines. We did not observe any significant change in the levels of several MICOS components tested (Mic19/CHCHD3, Mic60/Mitofilin and Mic25/ApooL). Outer mitochondrial membrane protein Sam50, known to closely associate to the MICOS complex to form the MIB complex and bridge the IMM and the OMM, also did not show any significant changes in DKO cells. In addition, we observed no changes in the levels of proteins related to Miro transport function (TRAK1 or TRAK2) or mitochondrial components like ATP5α or Tom20 (Fig. 1F). In contrast, we report a striking 4-fold increase in the levels of Inositol 1,4,5-trisphosphate (IP3) receptor (IP3R), a known regulator of the contact sites between ER and mitochondria that regulates Ca^{2+} communication between the two organelles (Fig. 1F). Other components of ERMCS that act in coordination with IP3R like GRP75 and the OMM channel VDAC1 were also found to be moderately upregulated, although not to a statistically significant level (Fig. 1F).

Loss of Miro1 and Miro2 alters ER/Mitochondrial communication

IP3Rs located at the ER are one of the main Ca^{2+}-release channels[44] and upon activation by Inositol 1,4,5-trisphosphate (IP3) can transfer Ca^{2+} to the mitochondria through a IP3R-VDAC complex[45]. In mammalian cells, IP3R acts as an adapter present on the ER that forms a complex with GRP75 and VDAC to maintain ERMCS[46]. At steady state, IP3R levels are tightly regulated and alteration of IP3R expression has been implicated with changes in ER morphology and ER Ca^{2+} release[47,48]. To study whether Miro accomplishes a role in regulating the connectivity of the ER membranes we performed a fluorescent recovery after photobleaching (FRAP) assay in our MEF cell lines. FRAP analysis of ER-luminal targeted DsRed (^{DsRed}ER) showed no significant difference in fluorescence recovery between WT and DKO cells (WT_M ~ 87 ± 7.5% against DKO_M ~86 ± 8.2 %), with just a delay in the initial recovery time (Fig. 2A and B; $t_{1/2}$ recovery time: 1.80 s ± 1.56-2.4 s for WT and 2.40 s ± 1.80-3.43 s for DKO; Median ± IQR, Mann–Whitney U test, p=0.019). This indicates that organelle connectivity of the ER remains overall constant upon loss of Miro.

ER-mitochondria contact sites are considered a dedicated molecular complex responsible for close contacts between both organelles with a prominent role in regulating Ca^{2+} communication between ER and mitochondria[39]. In addition, recent studies have demonstrated the presence of Gem1/dMiro at ER-mitochondria contact sites in yeast and *Drosophila*, respectively [15,16,42]. To test whether the increase in IP3R associates with changes in ERMCS in Miro DKO cells, we transfected WT and DKO cells with ^{GFP}Su9 and ^{DsRed}ER to label mitochondria and ER respectively and carried out deconvolution confocal microscopy to analyze the extent of ER and mitochondrial overlap. This analysis revealed that DKO cells showed a significant decrease in the overlapping area between ER and mitochondria (measured by Mander's coefficient) (Fig. 2C and D), which was specific to the loss of Miro as re-expression of either ^{Myc}Miro1 or ^{Myc}Miro2 in DKO cells rescued the amount of overlap between ER and mitochondria (Fig. 2C and D). This was further confirmed using TEM

by transfecting an ER-targeted HRP construct (KDEL-HRP)[49] to enhance the contrast of ER structures and allow the identification and quantification of ERMCS (defined by proximity of ER and mitochondria within 35 nm, Fig. 2E). DKO cells showed a decreased number of contacts between the two organelles (Fig. 2E and F; WT: 0.48 ± 0.19 and DKO: 0.36 ± 0.13; ER/mitochondria contacts; mean ± SD), confirming that Miro proteins accomplish a role in regulating ER and mitochondria association. To test if the altered ERMCS affects the communication between both the organelles, we measured mitochondrial Ca^{2+} uptake upon ATP induced Ca^{2+} release from ER stores (Fig. 2G). WT cells required 9.7s (9.73±0.75s, mean ± SEM) to reach maximum amplitude (F/F_{Min} = 1.44±0.03 fold mean ± SEM) while DKO cell showed a significantly delayed uptake (15.96±1.27s, mean ± SEM) and reduced amplitude (F/F_{Min} = 1.26±0.04, mean ± SEM) (Fig. 2G and H). This suggests that the ER/mitochondrial handling of Ca^{2+} is severely affected as a consequence of a decrease in ER/mitochondrial contact sites in DKO cells. We also observed that upon treatment with ATP, there was a significantly larger loss of Ca^{2+} from ER stores in DKO cells than in WT cells (Fig. 2G). This is probably due to increased level of IP3R receptors in DKO cells as more IP3R may result in a significantly larger Ca^{2+} release upon stimulation[48].

Miro proteins associate with MICOS components

Mitochondrial cristae are maintained by the interplay between the MICOS complex located at cristae junctions and Sam50 located at the OMM[50,51]. Alteration of MICOS complex proteins by knockout or knockdown has revealed their importance for the maintenance of mitochondrial cristae ultrastructure[51-53]. The disruption of cristae architecture in DKO MEFs (Fig. 1C and E) indicates a possible link between MICOS and Miro. Indeed, immunoprecipitation of ^{GFP}Miro1 and

^{GFP}Miro2 in HeLa cells revealed robust interactions with the core components of the MICOS complex Mic60/Mitofilin and Mic19/CHCHD3 and with the MIB complex forming component Sam50, whereas an unrelated OMM protein, Tom20, did not co-immunoprecipitate with either Miro1 or Miro2 (Fig. 3A). Interestingly, we did not detect interaction between Miro and Mitofusins or Mtx1, suggesting that these interactions might be low affinity, transient or cell type dependent (Fig. 3A). Control experiments with EGFP or the mitochondrially targeted ^{GFP}Su9 did not co-immunoprecipitate any of the MICOS components tested (Fig. 3A and Supplementary Fig. 2A and B) confirming the specificity of the interactions. Importantly, we confirmed endogenous association between Miro2 and Sam50 using specific antibodies against Miro2 in WT mouse brains, while as expected, anti-Miro2 antibodies did not co-immunoprecipitate Sam50 in brain lysates from Miro2 KO animals (Fig. 3B). Furthermore, Mic60/Mitofilin was also specifically co-immunoprecipitated with Miro2 in lysates from WT brains (Fig. 3B). We further confirmed the interaction of endogenous Miro2 with Sam50 and Mic60/Mitofilin *in situ* using a Proximity Ligation Assay (PLA), which allows to test association of proteins that reside in close proximity (30 - 40 nm) within the same complex[54]. In these experiments the presence of the antibody pair showed a 4-fold enrichment of fluorescent signals compared to the single antibodies confirming that native Miro2 and Sam50 as well as Miro2 and Mic19/CHCHD3 can be found in the same complex (Fig. 3C, with quantification shown in Fig. 3D and E). Moreover, Blue Native (BN)-PAGE followed by western blotting with Miro1 and Miro2 antibodies revealed the appearance of complexes at 1000 /1200 and 500 - 700 kDa that are similar to complexes detected with Mic19/CHCHD3, Sam50 or Mic60/Mitofilin antibodies (Fig. 3F)[50,53,55,56]. Thus, Miro proteins can be detected in a complex with key components of the MICOS complex on mitochondria.

Super-resolution imaging reveals that Miro is localized to discrete clusters on the mitochondrial surface

We noticed in our BN-PAGE experiments that both Miro1 and Miro2 antibodies detected strong and specific complexes around 140 kDa (Fig. 3G) both in HeLa cells and in MEFs suggesting that Miro1 and Miro2 could form dimers in the OMM. To further test this hypothesis, we co-transfected myc- and GFP- tagged versions of Miro1 and Miro2 and performed GFP-trap immunoprecipitations. Interestingly, we observed that Miro1 and Miro2 can interact with themselves and with each other thus indicating that the band around 140 kDa observed in the BN-PAGE gels might represent homodimers and/or heterodimers of both proteins (Fig. 4A). Thus, Miro proteins may form molecular platforms in the OMM upon which other mitochondrial molecular structures can be built. Using super-resolution imaging and immuno-gold labeling it has been shown that the MICOS complex can form an array that appears as 'discontinuous rail-like' structures[31]. Since Miro proteins interact with several MICOS components and loss of Miro results in cristae deformation, we investigated the sub-mitochondrial organization of Miro proteins and its relationship with the MICOS complexes. Diffraction-limited confocal microscopy revealed that either GFP- or Myc-tagged Miro proteins expressed in HeLa cells localized to the mitochondrial network as expected (Fig. 4B). Increasing the optical resolution two-fold by SIM imaging we observed that both Miro1 and Miro2 exhibited a discontinuous staining pattern on the mitochondrial membrane that was enriched in certain locations (Fig. 4B and Supplementary Fig. 3). SIM imaging revealed that in MEF cells, endogenous Miro2 proteins exhibited a similar discontinuous appearance confirming that native Miro proteins localize in discrete domains along the mitochondrial membrane (Supplementary Fig. 4). To investigate this further we took advantage of dSTORM[57-59] imaging (a super-resolution technique which provides almost six-fold higher

resolution than SIM) and performed correlative SIM / dSTORM[60]. Using dSTORM, we observed individually resolved clusters in ^{Myc}Miro1 expressing HeLa cells along the mitochondrial membrane that were not resolved under SIM imaging (Supplementary Fig. 5). Similar nanoclusters were also observed upon dSTORM imaging of ^{GFP}Miro1 or ^{GFP}Miro2 in HeLa cells (Fig. 4C). To confirm that cluster formation is not due to the use of dSTORM, we compared imaging of Miro proteins with mitochondrial matrix targeted ^{GFP}Su9 (as a negative control). In contrast to ^{GFP}Miro2, ^{GFP}Su9 showed a more uniform distribution in the mitochondria (Fig. 4C). To test whether the levels of Miro proteins on the mitochondrial membrane can influence cluster formation, we imaged HeLa cells expressing low to very high amounts of ^{GFP}Miro2 and observed that in all conditions ^{GFP}Miro2 formed similar clusters along mitochondria, confirming that Miro protein levels on the OMM do not play a significant role in this nanoscale organization (Supplementary Fig. 6). Further, we performed Density-Based Spatial Clustering of Applications with Noise (DBSCAN) which has been widely used to asses clustering of various membrane proteins[61]. The DBSCAN cluster map showed nanoscale domains formed by both ^{GFP}Miro1 and ^{GFP}Miro2 in Hela cells (Fig. 4D). We next quantified the sizes of Miro clusters by two complementary methods. First, we analyzed the cluster sizes using Ripley's K function[62] followed by quantification of cluster sizes post reconstruction of dSTORM images using the Feret's diameter (longest distance between any two points along the perimeter of each cluster). Ripley's K function indicated that both ^{GFP}Miro1 and ^{GFP}Miro2 formed a cluster size around 100-150 nm (Fig. 4E). The distribution of diameters revealed clusters ranging from 50 to 250 nm (Fig. 4F). ^{GFP}Miro1 clusters were found to have a median diameter around 100 nm (Median Feret's diameter = 108 nm ± 84-161 nm Interquartile Range (IQR)) very similar to that of ^{GFP}Miro2 clusters (Median Feret's diameter = 95 nm ± 67-150 nm (IQR)), both of which were much larger than the localization precision of the instrument

(marked as a red bar in Fig. 4F). To test whether the observed nanoscale distribution of the Miro clusters is specific to HeLa cells or conserved across different cell types, we also imaged ^{GFP}Miro2 clusters in our MEF cells and in primary cultures of hippocampal neurons. We observed nanocluster-like organization of ^{GFP}Miro2, similar to HeLa cells, in both MEFs and in primary hippocampal neurons (Supplementary Fig. 7A and B) demonstrating that the nanoscale distribution of Miro protein complexes appears to be conserved across cell types.

Miro nanodomains are closely associated with MICOS nanoclusters

Previous studies using super-resolution STED imaging revealed discontinuous clusters of MICOS proteins along mitochondria[31] similar to the Miro clusters we have described here. In conventional confocal imaging Miro and MICOS components exhibit homogeneous staining appearing to co-localize with each other (Supplementary Fig. 8A and B). To explore whether MICOS clusters are closely associated with Miro nanodomains, we performed dual color dSTORM with the known MICOS protein Mic60/Mitofilin. HeLa cells were transfected with ^{GFP}Miro2 and immunostained with an antibody against Mic60/Mitofilin. The nanoscale organization of Miro2 and Mic60/Mitofilin shared a similar distribution. Mic60/Mitofilin nanoclusters are regularly spaced and sparser than those observed for Miro, however, both sets of clusters appeared similar in size (Fig. 5A). Mic60/Mitofilin and Miro2 clusters were often present in close proximity to one another with partial overlap between them. The extent to which the two proteins co-cluster was calculated using Van Steensel's cross-correlation function (CCF)[63]. In HeLa cells labelled for Mic60/Mitofilin and Miro, the cross-correlation analysis showed a positive peak (Fig. 5D and E), indicating that both the clusters are positively correlated in the spatial domain. To test whether this correlation is specific, we transfected ^{GFP}Miro2 and labelled with anti-GFP antibody and a

nanobody against GFP conjugated to Alexa 647. The correlation analysis and mean CCF values showed a similar pattern to that obtained for Mic60/Mitofilin indicating that the correlation between Miro2 and Mitofilin is specific (Fig. 5B, D and E). Similar results were obtained when we calculated the Nearest Neighbor Distance (NND)[64] between Miro2 and Mic60/Mitofilin, which showed that Miro clusters and Mic60/Mitofilin clusters are localized adjacent to each other in a periodic manner (Supplementary Fig. 8C). Similarly, ^{GFP}Miro1 clusters also positively correlated with Mic60/Mitofilin clusters (Supplementary Fig. 8D and E). To test if the CCF was due to random localization, we performed a control experiment of dual color dSTORM with ^{GFP}Miro2 and Tom20 (previously shown to be non-interacting with Miro proteins). Figure 5E showed a significantly lower mean CCF between ^{GFP}Miro2 and Tom20 when compared to Miro2 and Mic60/Mitofilin (Fig. 5C, D and E) consistent with the specificity of the association between MICOS and Miro clusters.

Miro1 and Miro2 regulate MICOS complex formation and distribution

Our biochemical and super-resolution data revealed that Miro proteins form clusters in the mitochondrial surface that associate with MICOS clusters and interact with MICOS components and Sam50. In order to test whether Miro proteins are implicated in the correct association of the MICOS components we performed BN-PAGE on WT and DKO MEF cell lines. Miro1 antibodies detected specific bands from 500 to 700 kDa and around 1000 - 1200 kDa that were not present in DKO cells (Fig. 5F). These bands correlated with Mic19/CHCHD3 positive bands detected in WT cells supporting that Miro can form part of high order molecular complexes containing MICOS components. Interestingly, whilst the signal of Mic19/CHCHD3 positive complexes that migrated at around 500-700 kDa and 1200 kDa were reduced in DKO cells in comparison to WT (Fig. 5F),

a new molecular species positive for CHCHD3, appeared at a molecular weight of about 400 kDa in DKO lysates that was not present in WT cells (Fig. 5F), indicating that Miro proteins may be required for the correct assembly of MICOS complexes.

We aimed to understand whether the loss of Miro proteins affects the interaction between the core components of the MIB/MICOS complexes spanning OMM and IMM. Both Mic19/CHCHD3 and Sam50 pulled down the core components of MIB/MICOS, e.g. Mic60/Mitofilin, Mic19/CHCHD3 and Sam50 (Fig. 5G). These interactions appeared conserved in the absence of Miro (Fig. 5G) indicating that there is no gross alteration of the core MICOS complex. This was further investigated using PLA, which allows the *in situ* analysis of protein interactions. PLA analysis revealed that in absence of Miro there was a mild but significant decrease in the extent to which the core components of the MIB/MICOS interact (Fig. 5H and I). This weakening of interaction was consistent between Sam50 and Mic60/Mitofilin and between Mic60/Mitofilin and Mic19/CHCHD3 (Fig. 5H and I). Thus, while not essential for the assembly of MICOS complexes, Miro may regulate the overall stability of at least some species of these complexes, and its absence, leads to the destabilization of particular forms of the MICOS/MIB complexes.

Since Miro proteins can interact with several MICOS components and the depletion of Miro associates with defects in cristae architecture, we wanted to directly test how MICOS organization at the IMM is affected by the loss of Miro. We carried out dSTORM imaging after staining WT and DKO cells against the core MICOS component Mic19/CHCHD3. In WT cells Mic19/CHCHD3 showed an array of dense localizations evenly distributed throughout the entire mitochondria (Fig. 6A). In contrast, DKO cells showed mitochondrial regions with sporadic

localizations of Mic19/CHCHD3 (Fig. 6A). In addition, we carried out DBSCAN analysis which can reveal the extent of cluster formation from the raw localization data[61]. In WT MEFs, DBSCAN analysis revealed the previously reported formation of Mic60/Mitofilin clusters arranged in a "discontinuous rail-like distribution"[31] (Fig. 6A and B). Importantly, in DKO cells this array of clusters was severely affected, with large areas of mitochondria devoid of Mic19/CHCHD3 clusters (Red circles in Fig. 6B). This heterogeneity of Mic19/CHCHD3 clusters distribution correlated with altered Nearest Neighbor Distances (NND) distribution in DKO cells, compared to WT (Fig. 6C; $p < 0.001$, Two Sample KS test). In comparison to WT MEFs, DKO cells showed decreased shorter NND distances (~60-110 nm) while longer NND distances (>110 nm) were increased (Fig. 6C).

Miro proteins link the core MICOS complex to the microtubule transport machinery

MICOS cluster analysis in Miro DKO cells demonstrated that the distribution of MICOS clusters throughout the mitochondria is affected by the loss of Miro proteins. Due to its role in mitochondrial transport we hypothesized that Miro might well serve as a link between the MICOS clusters and the cytoskeleton. This link would ensure homogeneous distribution of MICOS throughout mitochondria and any alteration might result in deformed cristae architecture. To test this hypothesis, we performed immunoprecipitation assays from lysates from WT and Miro DKO cells with the core MICOS components and the two TRAK adaptor proteins. We observed a strong co-immunoprecipitation of TRAK1 when the IP was carried out with antibodies against Mic19/CHCHD3 or Sam50 (Fig. 6D). Strikingly, TRAK1 was no longer able to co-immunoprecipitate with Mic19/CHCHD3 or Sam50 in Miro DKO cells indicating that the interaction between TRAK1 and Mic19/CHCHD3 (and Sam50) is regulated by Miro (Fig. 6D).

TRAK2 was also observed to co-immunoprecipitate with MICOS components only in WT cells although to a lower extent than that of TRAK1 (Fig. 6D), further supporting the Miro-dependent interaction between TRAK1/2 and MICOS. Reciprocally, both Sam50 and Mic19/CHCHD3 were readily detected in immunoprecipitates using a TRAK1 antibody from WT lysates but not from DKO cell lysates (Fig. 6D). Thus, Miro maintains an association between the cristae structures and the motor machineries through a complex containing MIB/MICOS components and the TRAK motor adaptor proteins.

We have recently shown that TRAK proteins can localize to, and induce the anterograde trafficking of, mitochondria even in the absence of Miro[13]. The dependency on Miro of the TRAK1/MICOS association therefore, suggested that the transport machinery regulated by Miro ensures that the pulling forces generated by the motors are directly applied to the MIB/MICOS complexes to facilitate the concerted transport of both mitochondrial membranes. To test this we transfected our WT and DKO MEF cell lines with a version of GFP fused to the first 70 amino acids of Tom70 to target the protein to the OMM ($Tom70(1\text{-}70)^{GFP}$)[65] and co-labeled endogenous Mic19/CHCHD3 positive clusters with specific antibodies. Again, these experiments showed that the Mic19/CHCHD3 signal distributed heterogeneously in DKO cells with some mitochondria showing high density of Mic19/CHCHD3 signal together with other mitochondria showing very low signal (Fig. 6E). To force the uneven transport of membrane compartments in our MEF models, we expressed TRAK1 and the motor KIF5C (together with $Tom70(1\text{-}70)^{GFP}$ to label mitochondria) and observed that mitochondria accumulated in the periphery of the cells both in WT and in DKO cells as expected[13]. Strikingly, in WT cells the abundance of Mic19/CHCHD3 clusters matched the distal accumulation of mitochondria, showing higher signal in distally

transported mitochondria when compared with mitochondria that did not reach the periphery, thus suggesting that TRAK1/KIF5C directed trafficking co-transported Mic19/CHCHD3 positive clusters (Fig. 6F). In contrast, in the absence of the TRAK1 / MICOS bridge mediated by Miro, distally transported mitochondria were almost devoid of Mic19/CHCHD3 clusters in DKO cells (Fig. 6E and F) indicating that a critical role of Miro in regulating mitochondrial transport is to couple the TRAK/kinesin motor machineries to the MIB/MICOS complexes.

Miro regulated TRAK/MICOS bridge ensures appropriate distribution of inner components of mitochondria

The interaction between MICOS/Miro/TRAK carried an important implication. By linking the mitochondrial transport machinery to MICOS clusters Miro may ensure the concerted transport of the OMM with the IMM containing the complexes responsible for ATP generation. To test this hypothesis, we investigated the relative distribution of an IMM component of the OXPHOS system responsible for energy production (the ATPase subunit ATP5α) and an OMM protein, Tom40. We took advantage of our recently developed tools to accurately measure signal distribution in cells with restricted size and shape growing in adhesive micropatterned substrates (see Experimental procedures for details)[13,66]. We again forced the redistribution of mitochondria to the periphery of the cells by expressing TRAK1 and KIF5C and measured the relative distribution of Tom40 and ATP5α on mitochondria (Fig. 7). In WT cells both ATP5α and Tom40 signal presented a similar distribution in the mitochondrial network, consistent with a coordinated transport of both membranes (Fig. 7A and B). In stark contrast, DKO cells showed a relative accumulation of the OMM marker, Tom40, in the periphery of the cells while the ATP5α signal appeared more accumulated in more proximal structures (Fig. 7A and B). When we did the projection of all tips

of all 32 cells imaged (Fig. 7C and D) we noticed a consistent relative accumulation of the IMM marker (ATP5α) in the periphery of WT cells with respect to Tom40 signal, while in DKO cells the relative accumulation of the OMM marker in the periphery was accentuated (Fig. 7C and D). Further, we also measured the density of signal in mitochondria of ATP5α and Tom40 in concentric rings radiating out from the center of the cell (MitoSholl analysis)[13,67] and calculated the ratios of the normalized signals (ATP5α / Tom40) to plot them as a function of distance (Fig. 7E). The resulting plot shows that, in WT cells, the ATP5α / Tom40 ratio increases towards the periphery indicating that Miro-regulated TRAK1/KIF5C mitochondrial transport preferentially enriches the transported mitochondria with IMM components, perhaps by accumulating them by the pulling forces applied onto the MICOS complexes. In contrast, in DKO cells this ratio sharply drops in the most distal regions of the cell (Fig. 7E) indicating that, without Miro, TRAK directed mitochondrial transport fails to efficiently couple the IMM to the mitochondrial transport pathway. Altogether these results suggest that Miro acts as a critical adaptor to link the mitochondrial transport machinery to the mitochondrial cristae organization to ensure the concerted transport of the OMM with the IMM components to guarantee the appropriate provision of energy to the regions where mitochondria are delivered.

Discussion

Here we demonstrate the nanoscale spatial organization and protein complex formation of the Miro mitochondrial GTPases and their dual role in regulating the formation and functionality of the ERMCS and in connecting the MIB/MICOS complexes, responsible for maintaining cristae architecture, to the mitochondrial transport pathway. Miro proteins link the TRAK motor adaptors to the MICOS complexes to ensure the correct distribution of MICOS throughout the mitochondria and to facilitate the coordinated delivery of both membranes during mitochondrial transport.

ERMCS are key structures for the regulation of Ca^{2+} communication between ER and mitochondria and play important roles in the regulation of mitochondrial division and the segregation of mitochondria and mtDNA in newly generated mitochondrial tips[68]. In yeast, the Miro homolog Gem1 is associated with the regulation of ER-mitochondria connections[15]. In mammals, Miro interacts with Mitofusins and DISC1 which are known to be associated with ERMCS in mammalian cells[69-71]. Our data shows that, in addition, the absence of Miro proteins associates with a decrease in contacts between ER and mitochondria, which correlates with alterations in mitochondrial Ca^{2+} uptake and in the intraluminal concentration of Ca^{2+} in the ER. This role of Miro proteins in maintaining the ER-mitochondrial Ca^{2+} homeostasis is supported by recent reports that link dMiro to the control of the VDAC1-IP3R complexes that regulate Ca^{2+} communication in *Drosophila*[41,42]. Interestingly, the increase in the levels of IP3R that we report here are associated with alterations in Ca^{2+} homeostasis. Increased levels of IP3R have been previously associated with increased ER Ca^{2+} release which in turn has an impact on muscle contractility, induction of apoptosis and in the regulation of mitosis and that has been associated with multiple human diseases[72-75]. Altered Ca^{2+} communication between the ER and mitochondria

due to a decrease in ERMCS might be responsible for the increase in the protein levels of IP3R in Miro DKO cells. This provides striking evidence for the existence of a regulatory feedback mechanism that can control the number and composition of ER-mitochondrial contacts depending on the activity of the ERMCS complexes. It is worth noting that the upregulation of IP3R might be a direct result of altered ER-associated degradation (ERAD) at ERMCS[76]. IP3R levels are controlled by ubiquitination and the recent identification of the E3-ubiquitin ligase, Gp78, and other ERAD associated proteins at ERMCS suggests that loss of ERMCS might affect the ubiquitination and subsequent proteasomal degradation of IP3R[41,77]. Our results suggest that this regulatory mechanism may be controlled by the levels or activity of Miro proteins although further studies are needed to uncover the molecular targets of Miro regulation.

Combined loss of both Miro proteins disrupts the architecture of mitochondrial cristae. This effect is reminiscent of the impact of depleting MICOS complex components such as Mic60/Mitofilin, Mic19/CHCHD3 or some MICOS associated proteins[23,26,27,29,55,78,79]. Knockdown of Sam50, an OMM protein, also results in the loss of cristae structure pointing at the key role of the MIB and cross-talk between inner and outer mitochondrial membranes in regulating cristae architecture[24,51]. Our observations indicate a link between Miro and MIB/MICOS which was previously postulated by both genetic and mass spectrometric based screens[36,53]. Using super-resolution imaging we show that both Miro1 and Miro2 form nanoclusters of ~100 nm in size that are distributed throughout the mitochondrial network, reminiscent of clusters observed with MICOS proteins (Mic60/Mitofilin and Mic19/CHCHD3)[31]. Moreover, dual color dSTORM imaging indicates a close correlation in the distribution of Miro and MICOS protein clusters. Furthermore, we demonstrate that the loss of Miro proteins disrupts the previously reported

"discontinuous rail-like" distribution of MICOS complexes throughout mitochondria[31] as seen by the changes in our nearest-neighbor distances analysis.

The disruption of mitochondrial cristae architecture by loss of Miro, whilst widespread, does not perfectly match that observed upon deletion of MICOS components or Sam50, which are usually described as "onion-like" membranous structures[29]. Instead, the majority of mitochondria in Miro DKO cells presents large regions of mitochondria with low density of cristae which often appear vesiculated. Because proteins embedded in the environment of the phospholipid bilayer are dynamic and can diffuse laterally[80], Miro proteins might provide structural support to the MIB/MICOS complexes through the TRAK adaptor interaction. MIB/MICOS complexes that have lost the Miro/TRAK anchor might be subject to uncontrolled lateral diffusion in the OMM leading to the loss of their "discontinuous rail-like" distribution[31]. In addition, it is possible that MIB/MICOS complexes that are not anchored to the cytoskeleton are rendered less stable and dissociate to a certain extent, explaining why we observe a small but significant decrease in the interaction between core components of the MIB/MICOS complexes *in situ* in our PLA assays.

Miro proteins are critical regulators of mitochondrial trafficking from yeast to mammals[7]. The accepted model of mitochondrial trafficking presumed that Miro proteins provided a link between the OMM and the microtubule motors kinesin and dynein through the recruitment of the adaptors TRAK1 and TRAK2[81-84]. We have recently challenged this idea by showing that Miro is not essential for kinesin/TRAK directed mitochondrial movement but rather regulates its activity[13]. In the present paper we demonstrate that an important function of Miro proteins is to regulate the association of the mitochondrial transport machinery to the MICOS complexes. By regulating this

association, Miro proteins facilitate the concerted transport of both mitochondrial membranes to the cellular regions where they are needed. These findings are supported by a recent report linking Mic60/Mitofilin function, a core component of the MICOS complex, to mitochondrial motility in *Drosophila*[37]. Although the mechanism of such regulation remains unknown, in that work the authors report a decrease in dMiro levels upon genetic deletion of Mic60/Mitofilin. It remains to be tested if Miro is stabilized by the formation of assemblies between TRAK adaptors and MIB/MICOS complexes and whether the dissociation of these high order assemblies renders Miro prone to be degraded.

A major consequence of this regulation is that the mitochondrial cristae that are associated to the OMM through the MIB complexes could potentially be distributed in a regulated manner by the concerted action of Miro and TRAK proteins. Thus, by connecting the transport machinery to the MICOS complexes Miro opens the door to a new way of mitochondrial regulation by controlling the distribution of mitochondrial cristae within mitochondria. In addition, the direct association with the cristae molecular architecture may provide a mechanism for the transport machinery to sense the functionality of the mitochondria to be transported.

The dual role of Miro in regulating the number of ERMCS and the distribution of MIB/MICOS complexes has parallels with the ER–mitochondria organizing network (ERMIONE) in *Saccharomyces cerevisiae*[85,86]. ERMIONE in yeast is formed by ERMES (ER-Mitochondria Encounter Structure) and MICOS which then recruit the TOM complex and Sam50 and is involved in lipid homeostasis, mitochondrial biogenesis and maintenance of mitochondrial morphology[86]. However, there is little evidence of a structural molecular assembly in mammals that is

homologous to the yeast ERMIONE. Our work supports a central role for Miro proteins in coordinating and integrating different mitochondrial functions by organizing and controlling a mitochondrial signalling network that includes the mitochondrial transport pathway, the MIB/MICOS complexes and the ERMCS and that might be the functional equivalent of the ERMIONE in mammalian cells.

Materials and Methods

Plasmid DNA, Cell culture and transfection

^{GFP}Miro1 and ^{GFP}Miro2 were generated as described earlier[87] while ^{Myc}Miro1, ^{Myc}Miro2 and ^{Myc}Miro2ΔTM[12,88], ^{Myc}Mfn1[89] and ^{GFP}Su9 were obtained from Addgene. ^{GFP}TOM70(1-70) was generated in the lab by cloning the first 70 residues of TOM70 into EGFP-N1 vector[65]. HeLa and HEK293T cells were cultured in DMEM medium (Gibco) supplemented with streptomycin (100 µg/ml), penicillin (100 U/ml), and 10% fetal bovine serum in a 10 cm cell culture dishes while 15% fetal bovine serum was used to culture Mouse Embryonic Fibroblast cells. Cells were transfected with ~5 µg plasmid DNA using nucleofection (Amaxa, Lonza AG) according to manufacturer's protocol. Rat hippocampal cultures were prepared as described earlier [90-92] and transfected at 7-9 DIV using Lipofectamine®2000.

Immunostaining and biochemical assays

24 h post transfection, cells were fixed with 4% PFA at 37^{o}C for 10 min, washed and coverslips were incubated for 30-45 min in blocking solution. Coverslips were then incubated with primary antibodies (see Supplementary Table 1 and Supplementary Materials and Methods for details) followed by secondary antibodies diluted in blocking solution and extensive washing to remove free fluorophores. Coverslips were further fixed for 8 min in 4% PFA, washed and mounted for imaging.

For co-immunoprecipitation experiments in HeLa cells, cells were lysed 24 h post transfection in lysis buffer (50 mM Tris pH 7.5; 0.5% Triton; 150 mM NaCl; 1 mM EDTA and 1 mM PMSF) containing protease inhibitors. The lysed samples were incubated with GFP-TRAP beads

(Chromotek GmBH) for 1 hour. Complexes were then washed several times and eluted with 3× Laemmli sample buffer and western blotted on nitrocellulose membrane.

Co-immunoprecipitation experiments in MEF cells and in brains were performed similarly. Cells were collected and washed in PBS by centrifugation or adult brains were dissected prior to homogenization with lysis buffer (50 mM HEPES pH 7.5; 0.5% Triton; 150 mM NaCl; 1 mM EDTA and 1 mM PMSF) containing protease inhibitors. Homogenates were cleared by centrifugation at 38.000 rpm for 40 minutes. 1 μg of antibody was added to 1 ml of samples containing 2 mg of protein and incubated in rotation overnight at 4^{o}C. The next day a mix 1:1 of ProtA and ProtG coated agarose beads were blocked in lysis buffer containing 3 mg/ml of BSA for 1 hour. After washing in lysis buffer 20 μl of the beads mix was added to every tube and incubated for one hour. Beads were then washed several times in lysis buffer and resuspended in Laemmli buffer, boiled for 5 minutes a kept at -20^{o}C until ran in acrylamide gels.

BN-PAGE was performed using NativePAGE™ Bis-Tris Gel System from Life technologies. Proximity Ligation Assay was performed with Duolink® In Situ Red PLA reagents according to manufacturer's protocol (Sigma Aldrich)[70,93].

Confocal, SIM, correlated SIM, dSTORM and 3D dSTORM imaging

Confocal imaging was performed on a Zeiss LSM 700 confocal microscope, Structured Illumination Microscopy was performed on Zeiss Elyra PS.1, correlated SIM and dSTORM imaging was performed on the same microscope with 100 × 1.46 NA oil immersion objective. All dSTORM imaging was conducted using a custom-built microscope and analyzed using software written in C++ and Python[94]. Further details about microscopes used in this study can be found in supplementary experimental procedures.

Image processing and analysis

Post reconstruction, images were first corrected for X-Y drift using 1 to 3 fiducials present in the images. Images were either binned using 20 nm pixel size (for dSTORM and colocalization with MICOS components) or 30 nm pixel size (for dimer formation). The reconstructed image was blurred with a Gaussian function with a sigma radius of 0.75 (which translate to 20-30 nm) using 'Accurate Gaussian blur' plugin. For measuring the sizes of nanoclusters, first images were thresholded, and then each particle was detected using particle analyzer algorithm followed by particle size measurement using Feret's diameter plugin present in ImageJ. For colocalization of dual color STORM images, images in 555 nm and 647 nm channels were blurred equally then both channels were aligned using 'Align images FFT' plugin present within GDSC ImageJ plugin (freely downloadable from University of Sussex) which uses a Gaussian for sub-pixel alignment. Van steensel's cross correlation was calculated from the aligned images using plugin JACoP with X-shift of 1 μm. DBSCAN and Ripley's K function was determined according to a previously published protocol[95].

Statistical Analysis

Excel Software (Microsoft), Origin (OriginLab Corporation) and GraphPad Prism (GraphPad Software, Inc) were used to analyze the data. Statistical significance was calculated using either Student's t- test or Mann–Whitney U test (for non-parametric two independent samples) unless otherwise stated. Statistical differences between multiple conditions were performed by one- way ANOVA followed by post hoc Tukey's tests (for comparison between two conditions) or Bonferroni test (for comparison between multiple conditions). Statistical significance was pre-

fixed at $P < 0.05$, described as $*P < 0.05$; $**P < 0.01$ and $***P < 0.001$. All values in text are given as Mean ± S.E.M unless specified.

Acknowledgments

This work was supported by an ERC starting grant (282430) and Lister Institute for Preventive Medicine prize to J.T.K. A.R.L. acknowledges support from the Medical Research Council award MR/K015826/1. S.M. was supported by an EMBO Long-Term Fellowship and Marie Skłodowska-Curie International Incoming Fellowship (No. 630033 and 913033). J.J.B. is supported by core funding to the MRC_UCL LMCB University Unit (Grant ref. MC_U12266B). E.F.H. received funding from the European Union's Horizon 2020 research and innovation programme under the Marie Skłodowska-Curie (No. 661733). D.I. was supported by an Institute of Neurology Clinical Neuroscience PhD and C.C-C. by the MRC LMCB PhD programme. J.T.K and S.M. acknowledge support from the UCL super-resolution facility for the use of Zeiss Elyra PS.1 microscope and image analysis platform.

Figure legends

Figure 1: Loss of Miro is associated with altered cristae morphology. (A) Imaging of mitochondrial matrix with $mtRo^{GFP}$. WT and Miro DKO MEF cells were transfected with the mitochondrial matrix targeted $mtRo^{GFP}$ and imaged using Structured Illumination Microscopy (SIM). (B) Quantification of the images shown in (A) by scoring abnormalities in matrix continuity revealed by GFP in WT, DKO and DKO cells re-expressing Miro proteins (WT and DKO cells: n >30, Miro re-expressing cells: n >20 cells, $p < 0.05$ (Student's t-test)). (C) TEM images of mitochondrial cristae morphologies observed in WT and Miro DKO MEFs. (D) Quantification of TEM images after classification of the cells as having normal cristae morphology or an altered cristae morphology (>35 cells for each genotype were analyzed from 2 independent sample preparations; $p< 0.001$ (Student's t-test)). (E) Representative EM images of mitochondria from WT and DKO cells showing the homogeneity of cristae in WT cells and the appearance of spaces and enlargement of mitochondrial units in regions without cristae in DKO cells. (F) Western blot analysis and quantification of 3 different cell lines independently generated for each genotype (3 for WT and 3 for DKO) to analyze cellular levels of proteins related to the cytoskeleton, MICOS complex and ERMCS.

Figure 2: Miro protein regulate ER/Mitochondrial communication by regulating the number of ER/Mitochondria Contact Sites (ERMCS).

(A) FRAP analysis of ER dynamics measured in MEF cells. WT and DKO cells were transfected with ^{DsRed}ER and FRAP was performed using a spinning disk confocal microscope. (B) Quantification of images shown in (A). Inset: Expanded region of first 12s of the recovery after bleaching is quantified (n>30 cells; $p < 0.05$ (One-Way ANOVA)). (C) Representative images of MEF cells expressing ^{GFP}Su9 and ^{DsRed}ER that were imaged live in a spinning disk confocal microscope. (D) Quantification of Mander's coefficient between ER and Mitochondria from (C) (n>20 cells; $p < 0.001$ (One-Way ANOVA)). (E) Electron micrographs of mitochondria and ER in WT and DKO cells expressing an HRP construct fused to an ER retention signal (KDEL). The oxidation of DAB (3,3'-Diaminobenzidine) driven by HRP produces an electron-dense precipitate that is retained in the lumen of the ER increasing the contrast of ER tubules in the cytoplasm. Yellow asterisks depict mitochondria; red arrows point to ER/mitochondria close contacts (<35nm). A magnified view of close contacts between ER and mitochondria obtained from the boxed region in the WT image is also shown. (F) Quantification of close contacts between two organelles in TEM images from WT and DKO cells (n>20 cells for each genotype; WT >400 and DKO >700 mitochondria; from 2 independent sample preparations; $p < 0.05$, One-Way ANOVA). (G) Agonist induced Ca^{2+} release from ER and subsequent mitochondrial Ca^{2+} uptake. Arrow indicates addition of agonist ATP. (H) Rise time (Calculated from baseline to maximum amplitude after addition of ATP) in WT and DKO cells (n>30 cells, $p <0.001$, One-Way ANOVA).

Figure 3: Miro proteins are a component of the MICOS complex.

(A) Miro proteins interact with MICOS complex proteins. Western blot analysis of ^{GFP}Miro protein complexes from HeLa cells were analyzed in SDS-PAGE for several MICOS components. (B) Co-immunoprecipitation of Miro2 with endogenous MICOS complex proteins. Immunoprecipitation was performed from WT and Miro2 KO brains and western blot was performed with different antibodies against MICOS complex proteins. Approximately 2% of total cell lysate used for immunoprecipitation was loaded for inputs. (C) Proximity Ligation Assay (PLA) between Miro2 and OMM protein Sam50 (Top panel) as well as PLA between Miro2 and the MICOS specific protein Mic19/CHCHD3 (Bottom panel). Nucleus is shown in blue (DAPI) and PLA assay products are shown in red. (D, E) Quantification of the experiments shown in (C). (F) Blue Native PAGE (BN-PAGE) of total HeLa cell lysate was prepared, resolved on Bis-Tris polyacrylamide gels and western blotting was performed using various antibodies. Molecular complexes of Miro proteins and MICOS complexes are marked with arrows. (G) BN-PAGE followed by western blot with Miro antibody from HeLa, WT and DKO MEFs. Only 60 kDa to 240 kDa region is shown.

Figure 4: Sub-organellar localization of Miro proteins in mitochondria.

(A) Western blot analysis of Miro1 and Miro2 interaction. HeLa cells were transfected with GFP as a control or ^{GFP}Miro 1/2 and ^{Myc}Miro1/2. Immunoprecipitation was carried out using GFP trap agarose beads and immunoblotted with GFP and Myc antibodies. (B) Widefield TIRF image of a representative HeLa cell overexpressing ^{Myc}Miro1 and immunostained with anti-Myc antibody. Inset shows the super-resolution image after structured illumination (SIM). (C) dSTORM image of HeLa cells transfected with ^{GFP}Miro1, ^{GFP}Miro2 or ^{GFP}Su9. Both Miro1 and Miro2 localize to nanometer sized clusters on the mitochondrial surface. (D) Density-based spatial clustering of applications with noise (DBSCAN) analysis of ^{GFP}Miro1 and ^{GFP}Miro2. Clustered localizations are represented by pseudo color-coding with localizations that are non-clustered is represented as gray pixels. (E) Mean Ripley's K-function analysis of ^{GFP}Miro1 (Red) and ^{GFP}Miro2 (Black). Transformed K-function (L(r)-r) is represented against increasing cluster radius. The homogeneous Poisson distribution of the localizations is shown in Blue. Three independent experiments, n>6 cells. (F) Size distribution of clusters formed by ^{GFP}Miro1 and ^{GFP}Miro2 respectively in HeLa cells. After reconstruction of dSTORM images, Mean Feret's diameter was measured using ImageJ and plotted. Red line represents localization precision of the dSTORM setup. Three independent measurements, n>7 cells.

Figure 5: Miro nanodomains associate with MICOS clusters.

(A-C) Dual color dSTORM imaging of ^{GFP}Miro2 transfected HeLa cells. ^{GFP}Miro2 nanometer sized domains are shown (anti-GFP - green) together with endogenous Mic60/Mitofilin (A) a positive control for Miro2 (B - anti-Miro2 antibody) and negative control for Tom20 (C). (D) Cross-correlation analysis between Miro2 and Mic60; Miro2 and ^{GFP}Miro2 and Miro2 and Tom20. (E) Mean Van-Steensel's cross correlation coefficient between ^{GFP}Miro2 and the different immunostainings are calculated from (D) and plotted. Three independent measurements were performed. $n \geq 5$ cells (One-Way ANOVA). (F) BN-PAGE of Miro and Mic19/CHCHD3 protein complexes in WT and DKO MEF cells revealing the Miro specificity of the complexes ("*" indicates unspecific band). Arrows indicate molecular weight of MICOS complexes (revealed with CHCHD3 antibody). "**" indicates a new species of MICOS positive complex appearing due to the loss of Miro. (G) Endogenous immunoprecipitation experiment in WT and DKO cells using antibodies against the core forming MICOS components (Mic19/CHCHD3, Mic60/Mitofilin and Sam50). The main interactions are not to be critically affected. (H and I) Proximity Ligation Assay (PLA) and quantification in WT and DKO cells between Sam50 and Mic60/Mitofilin (H) and between Mic60/Mitofilin and Mic19/CHCHD3 (I) shows mild decrease in the association between these components. Data from three independent experiments, (One-Way ANOVA). Significance: * $p < 0.05$; ** $p < 0.01$; *** $p < 0.001$

Figure 6: Distribution of MICOS clusters is altered in Miro DKO cells due to the loss of cytoskeletal anchorage.

(A) Distribution of MICOS (Mic19/CHCHD3) clusters along the mitochondrial membrane in WT and DKO cells. Pseudo-colored representation of reconstructed dSTORM images of MICOS complexes. (B) DBSCAN cluster map of Mic19/CHCHD3 clusters. DKO cells show areas with depletion of clusters in comparison to WT cells. (C) Quantification of nearest neighbor distances between MICOS clusters present in WT and DKO cells. Histogram of all the observed distances between MICOS clusters are shown. WT: 8 cells, DKO: 11 cells comprising >30000 NND. (C) Endogenous immunoprecipitation experiment in WT and DKO cells using antibodies against the core forming MICOS components (Mic19/CHCHD3, Mic60/Mitofilin and Sam50) and antibodies against the TRAK motor adaptors. TRAK proteins interact with critical MICOS components in a Miro dependent manner. (D) Mic19/CHCHD3 positive MICOS clusters in WT distribute homogeneously in the mitochondrial population in WT MEFs while the loss of Miro proteins correlates with an increase in heterogeneity in the distribution, with cells showing mitochondrial units almost devoid of Mic19/CHCHD3 signal (white arrows). (E) Overexpressing TRAK1 and KIF5C induces the redistribution of mitochondria to the periphery. In WT cells this redistribution correlates with increased Mic19/CHCHD3 signal in the periphery (cyan arrows). In DKO cells TRAK1/KIF5C redistribution enhances the heterogeneity of Mic19/CHCHD3 staining indicating a transport-mediated uncoupling of OMM and IMM in Miro DKO cells. Mitochondria with low Mic19/CHCHD3 signal concentrates in the TRAK1/KIF5C anterogradely transported mitochondria (white arrows) while Mic19/CHCHD3 signal accumulate in proximal - not transported - mitochondria (cyan arrows).

Figure 7: Miro links the microtubule transport pathway to the MICOS complex through TRAK

(A) Quantification of the distribution of OMM and IMM components upon TRAK1/KIF5C overexpression in micropatterned substrates. WT and MiroDKO cells expressing the Tom70(1-70)^{GFP} together with the mitochondrial motor machinery TRAK1/KIF5C were grown in "Y"-shaped micropatterns to produce triangular cells. Cells were immunostained for endogenous expression of an OMM marker (Tom40 - cyan) and an IMM marker (ATP5α - red). (B) Cell representations of the relative accumulations of the OMM marker Tom40 (subtraction of the ATP5α signal from the Tom40 signal; upper row) and the IMM marker ATP5α (subtraction of the Tom40 signal from the ATP5α signal, bottom row). (C) Projections of all the 76 cell tips that contained mitochondria and generation of mitochondrial probability maps. In WT cells both OMM and IMM markers are similarly distributed while in the Miro DKO cells the OMM marker is preferentially accumulated in the most distal regions compared to the IMM which accumulates in more proximal regions. (D) Projections from the 76 subtracted images (for each genotype) were generated as in (B). (E) Mitochondrial Probability Map to quantify the ratio between the normalized signals of OMM (Tom40) and IMM (ATP5α) components as a function of the distance from the center of the cell. (See Supplementary experimental procedures for details). All experiments were performed at least 3 independent times. Quantification and statistics in (E) were performed with 32 cells for each genotype (n = cells).

Significance: * $p < 0.05$; ** $p < 0.01$ and *** $p < 0.001$

References

1 Tait, S. W. & Green, D. R. Mitochondria and cell signalling. *Journal of cell science* **125**, 807-815, doi:10.1242/jcs.099234 (2012).

2 Cockrell, R. S., Harris, E. J. & Pressman, B. C. Synthesis of ATP driven by a potassium gradient in mitochondria. *Nature* **215**, 1487-1488 (1967).

3 Wikstrom, M. K. Proton pump coupled to cytochrome c oxidase in mitochondria. *Nature* **266**, 271-273 (1977).

4 Rizzuto, R., De Stefani, D., Raffaello, A. & Mammucari, C. Mitochondria as sensors and regulators of calcium signalling. *Nature reviews. Molecular cell biology* **13**, 566-578, doi:10.1038/nrm3412 (2012).

5 Macaskill, A. F. *et al.* Miro1 is a calcium sensor for glutamate receptor-dependent localization of mitochondria at synapses. *Neuron* **61**, 541-555, doi:10.1016/j.neuron.2009.01.030 (2009).

6 Orrenius, S., Gogvadze, V. & Zhivotovsky, B. Mitochondrial oxidative stress: implications for cell death. *Annu Rev Pharmacol Toxicol* **47**, 143-183, doi:10.1146/annurev.pharmtox.47.120505.105122 (2007).

7 Birsa, N., Norkett, R., Higgs, N., Lopez-Domenech, G. & Kittler, J. T. Mitochondrial trafficking in neurons and the role of the Miro family of GTPase proteins. *Biochemical Society transactions* **41**, 1525-1531, doi:10.1042/BST20130234 (2013).

8 Brickley, K., Smith, M. J., Beck, M. & Stephenson, F. A. GRIF-1 and OIP106, members of a novel gene family of coiled-coil domain proteins: association in vivo and in vitro with kinesin. *The Journal of biological chemistry* **280**, 14723-14732, doi:10.1074/jbc.M409095200 (2005).

9 Brickley, K. & Stephenson, F. A. Trafficking kinesin protein (TRAK)-mediated transport of mitochondria in axons of hippocampal neurons. *The Journal of biological chemistry* **286**, 18079-18092, doi:10.1074/jbc.M111.236018 (2011).

10 Wang, X. & Schwarz, T. L. The mechanism of Ca2+ -dependent regulation of kinesin-mediated mitochondrial motility. *Cell* **136**, 163-174, doi:10.1016/j.cell.2008.11.046 (2009).

11 Stowers, R. S., Megeath, L. J., Gorska-Andrzejak, J., Meinertzhagen, I. A. & Schwarz, T. L. Axonal transport of mitochondria to synapses depends on milton, a novel Drosophila protein. *Neuron* **36**, 1063-1077 (2002).

12 Fransson, S., Ruusala, A. & Aspenstrom, P. The atypical Rho GTPases Miro-1 and Miro-2 have essential roles in mitochondrial trafficking. *Biochem Biophys Res Commun* **344**, 500-510 (2006).

13 Lopez-Domenech, G. *et al.* Miro proteins coordinate microtubule- and actin-dependent mitochondrial transport and distribution. *The EMBO journal* **37**, 321-336, doi:10.15252/embj.201696380 (2018).

14 Oeding, S. J. *et al.* Identification of Miro1 and Miro2 as mitochondrial receptors for myosin XIX. *Journal of cell science* **131**, doi:10.1242/jcs.219469 (2018).

15 Kornmann, B., Osman, C. & Walter, P. The conserved GTPase Gem1 regulates endoplasmic reticulum-mitochondria connections. *Proceedings of the National Academy of Sciences of the United States of America* **108**, 14151-14156, doi:10.1073/pnas.1111314108 (2011).

16 Stroud, D. A. *et al.* Composition and topology of the endoplasmic reticulum-mitochondria encounter structure. *Journal of molecular biology* **413**, 743-750, doi:10.1016/j.jmb.2011.09.012 (2011).

17 Murley, A. *et al.* ER-associated mitochondrial division links the distribution of mitochondria and mitochondrial DNA in yeast. *Elife* **2**, e00422, doi:10.7554/eLife.00422 (2013).

18 Guo, X. *et al.* The GTPase dMiro is required for axonal transport of mitochondria to Drosophila synapses. *Neuron* **47**, 379-393, doi:10.1016/j.neuron.2005.06.027 (2005).

19 Pfanner, N. *et al.* Uniform nomenclature for the mitochondrial contact site and cristae organizing system. *J Cell Biol* **204**, 1083-1086, doi:10.1083/jcb.201401006 (2014).

20 von der Malsburg, K. *et al.* Dual role of mitofilin in mitochondrial membrane organization and protein biogenesis. *Dev Cell* **21**, 694-707, doi:10.1016/j.devcel.2011.08.026 (2011).

21 Zerbes, R. M. *et al.* Mitofilin complexes: conserved organizers of mitochondrial membrane architecture. *Biol Chem* **393**, 1247-1261, doi:10.1515/hsz-2012-0239 (2012).

22 Bohnert, M. *et al.* Role of mitochondrial inner membrane organizing system in protein biogenesis of the mitochondrial outer membrane. *Molecular biology of the cell* **23**, 3948-3956, doi:10.1091/mbc.E12-04-0295 (2012).

23 An, J. *et al.* CHCM1/CHCHD6, novel mitochondrial protein linked to regulation of mitofilin and mitochondrial cristae morphology. *The Journal of biological chemistry* **287**, 7411-7426, doi:10.1074/jbc.M111.277103 (2012).

24 Ott, C. *et al.* Sam50 functions in mitochondrial intermembrane space bridging and biogenesis of respiratory complexes. *Molecular and cellular biology* **32**, 1173-1188, doi:10.1128/MCB.06388-11 (2012).

25 Xie, J., Marusich, M. F., Souda, P., Whitelegge, J. & Capaldi, R. A. The mitochondrial inner membrane protein mitofilin exists as a complex with SAM50, metaxins 1 and 2, coiled-coil-helix coiled-coil-helix domain-containing protein 3 and 6 and DnaJC11. *FEBS letters* **581**, 3545-3549, doi:10.1016/j.febslet.2007.06.052 (2007).

26 Weber, T. A. *et al.* APOOL is a cardiolipin-binding constituent of the Mitofilin/MINOS protein complex determining cristae morphology in mammalian mitochondria. *PloS one* **8**, e63683, doi:10.1371/journal.pone.0063683 (2013).

27 Darshi, M. *et al.* ChChd3, an inner mitochondrial membrane protein, is essential for maintaining crista integrity and mitochondrial function. *The Journal of biological chemistry* **286**, 2918-2932, doi:10.1074/jbc.M110.171975 (2011).

28 Yang, R. F. *et al.* Suppression of Mic60 compromises mitochondrial transcription and oxidative phosphorylation. *Sci Rep* **5**, 7990, doi:10.1038/srep07990 (2015).

29 John, G. B. *et al.* The mitochondrial inner membrane protein mitofilin controls cristae morphology. *Molecular biology of the cell* **16**, 1543-1554, doi:10.1091/mbc.e04-08-0697 (2005).

30 Rabl, R. *et al.* Formation of cristae and crista junctions in mitochondria depends on antagonism between Fcj1 and Su e/g. *J Cell Biol* **185**, 1047-1063, doi:10.1083/jcb.200811099 (2009).

31 Jans, D. C. *et al.* STED super-resolution microscopy reveals an array of MINOS clusters along human mitochondria. *Proceedings of the National Academy of Sciences of the United States of America* **110**, 8936-8941, doi:10.1073/pnas.1301820110 (2013).

32 Rampelt, H., Zerbes, R. M., van der Laan, M. & Pfanner, N. Role of the mitochondrial contact site and cristae organizing system in membrane architecture and dynamics.

Biochim Biophys Acta Mol Cell Res **1864**, 737-746, doi:10.1016/j.bbamcr.2016.05.020 (2017).

33 Friedman, J. R., Mourier, A., Yamada, J., McCaffery, J. M. & Nunnari, J. MICOS coordinates with respiratory complexes and lipids to establish mitochondrial inner membrane architecture. *Elife* **4**, doi:10.7554/eLife.07739 (2015).

34 Ott, C., Dorsch, E., Fraunholz, M., Straub, S. & Kozjak-Pavlovic, V. Detailed analysis of the human mitochondrial contact site complex indicate a hierarchy of subunits. *PloS one* **10**, e0120213, doi:10.1371/journal.pone.0120213 (2015).

35 Kozjak-Pavlovic, V. The MICOS complex of human mitochondria. *Cell Tissue Res* **367**, 83-93, doi:10.1007/s00441-016-2433-7 (2017).

36 Hoppins, S. *et al.* A mitochondrial-focused genetic interaction map reveals a scaffold-like complex required for inner membrane organization in mitochondria. *J Cell Biol* **195**, 323-340, doi:10.1083/jcb.201107053 (2011).

37 Tsai, P. I., Papakyrikos, A. M., Hsieh, C. H. & Wang, X. Drosophila MIC60/mitofilin conducts dual roles in mitochondrial motility and crista structure. *Molecular biology of the cell* **28**, 3471-3479, doi:10.1091/mbc.E17-03-0177 (2017).

38 Kornmann, B. *et al.* An ER-mitochondria tethering complex revealed by a synthetic biology screen. *Science* **325**, 477-481, doi:10.1126/science.1175088 (2009).

39 Rowland, A. A. & Voeltz, G. K. Endoplasmic reticulum-mitochondria contacts: function of the junction. *Nature reviews. Molecular cell biology* **13**, 607-625, doi:10.1038/nrm3440 (2012).

40 Hamasaki, M. *et al.* Autophagosomes form at ER-mitochondria contact sites. *Nature* **495**, 389-393, doi:10.1038/nature11910 (2013).

41 Lee, K. S. *et al.* Altered ER-mitochondria contact impacts mitochondria calcium homeostasis and contributes to neurodegeneration in vivo in disease models. *Proceedings of the National Academy of Sciences of the United States of America* **115**, E8844-E8853, doi:10.1073/pnas.1721136115 (2018).

42 Lee, S. *et al.* Polo Kinase Phosphorylates Miro to Control ER-Mitochondria Contact Sites and Mitochondrial Ca(2+) Homeostasis in Neural Stem Cell Development. *Dev Cell* **37**, 174-189, doi:10.1016/j.devcel.2016.03.023 (2016).

43 Gustafsson, M. G. Surpassing the lateral resolution limit by a factor of two using structured illumination microscopy. *J Microsc* **198**, 82-87 (2000).

44 Patterson, R. L., Boehning, D. & Snyder, S. H. Inositol 1,4,5-trisphosphate receptors as signal integrators. *Annu Rev Biochem* **73**, 437-465, doi:10.1146/annurev.biochem.73.071403.161303 (2004).

45 Decuypere, J. P. *et al.* IP(3) Receptors, Mitochondria, and Ca Signaling: Implications for Aging. *J Aging Res* **2011**, 920178, doi:10.4061/2011/920178 (2011).

46 Szabadkai, G. *et al.* Chaperone-mediated coupling of endoplasmic reticulum and mitochondrial Ca2+ channels. *J Cell Biol* **175**, 901-911, doi:10.1083/jcb.200608073 (2006).

47 Takei, K., Mignery, G. A., Mugnaini, E., Sudhof, T. C. & De Camilli, P. Inositol 1,4,5-trisphosphate receptor causes formation of ER cisternal stacks in transfected fibroblasts and in cerebellar Purkinje cells. *Neuron* **12**, 327-342 (1994).

48 Sampieri, A., Santoyo, K., Asanov, A. & Vaca, L. Association of the IP3R to STIM1 provides a reduced intraluminal calcium microenvironment, resulting in enhanced store-operated calcium entry. *Sci Rep* **8**, 13252, doi:10.1038/s41598-018-31621-0 (2018).

49 Connolly, C. N., Futter, C. E., Gibson, A., Hopkins, C. R. & Cutler, D. F. Transport into and out of the Golgi complex studied by transfecting cells with cDNAs encoding horseradish peroxidase. *J Cell Biol* **127**, 641-652 (1994).

50 Huynen, M. A., Muhlmeister, M., Gotthardt, K., Guerrero-Castillo, S. & Brandt, U. Evolution and structural organization of the mitochondrial contact site (MICOS) complex and the mitochondrial intermembrane space bridging (MIB) complex. *Biochimica et biophysica acta* **1863**, 91-101, doi:10.1016/j.bbamcr.2015.10.009 (2016).

51 Ding, C. *et al.* Mitofilin and CHCHD6 physically interact with Sam50 to sustain cristae structure. *Sci Rep* **5**, 16064, doi:10.1038/srep16064 (2015).

52 Anand, R., Strecker, V., Urbach, J., Wittig, I. & Reichert, A. S. Mic13 Is Essential for Formation of Crista Junctions in Mammalian Cells. *PloS one* **11**, e0160258, doi:10.1371/journal.pone.0160258 (2016).

53 Guarani, V. *et al.* QIL1 is a novel mitochondrial protein required for MICOS complex stability and cristae morphology. *Elife* **4**, doi:10.7554/eLife.06265 (2015).

54 Soderberg, O. *et al.* Direct observation of individual endogenous protein complexes in situ by proximity ligation. *Nat Methods* **3**, 995-1000, doi:10.1038/nmeth947 (2006).

55 Pinero-Martos, E. *et al.* Disrupted in schizophrenia 1 (DISC1) is a constituent of the mammalian mitochondrial contact site and cristae organizing system (MICOS) complex, and is essential for oxidative phosphorylation. *Hum Mol Genet* **25**, 4157-4169, doi:10.1093/hmg/ddw250 (2016).

56 Plecita-Hlavata, L. *et al.* Hypoxic HepG2 cell adaptation decreases ATP synthase dimers and ATP production in inflated cristae by mitofilin down-regulation concomitant to MICOS clustering. *FASEB J* **30**, 1941-1957, doi:10.1096/fj.201500176 (2016).

57 Rust, M. J., Bates, M. & Zhuang, X. Sub-diffraction-limit imaging by stochastic optical reconstruction microscopy (STORM). *Nat Methods* **3**, 793-795, doi:10.1038/nmeth929 (2006).

58 Huang, B., Jones, S. A., Brandenburg, B. & Zhuang, X. Whole-cell 3D STORM reveals interactions between cellular structures with nanometer-scale resolution. *Nat Methods* **5**, 1047-1052, doi:10.1038/nmeth.1274 (2008).

59 van de Linde, S., Sauer, M. & Heilemann, M. Subdiffraction-resolution fluorescence imaging of proteins in the mitochondrial inner membrane with photoswitchable fluorophores. *J Struct Biol* **164**, 250-254, doi:10.1016/j.jsb.2008.08.002 (2008).

60 Hamel, V. *et al.* Correlative multicolor 3D SIM and STORM microscopy. *Biomed Opt Express* **5**, 3326-3336, doi:10.1364/BOE.5.003326 (2014).

61 Rahbek-Clemmensen, T. *et al.* Super-resolution microscopy reveals functional organization of dopamine transporters into cholesterol and neuronal activity-dependent nanodomains. *Nature communications* **8**, 740, doi:10.1038/s41467-017-00790-3 (2017).

62 Yan, Q. *et al.* Mechanistic insights into GLUT1 activation and clustering revealed by super-resolution imaging. *Proceedings of the National Academy of Sciences of the United States of America* **115**, 7033-7038, doi:10.1073/pnas.1803859115 (2018).

63 van Steensel, B. *et al.* Partial colocalization of glucocorticoid and mineralocorticoid receptors in discrete compartments in nuclei of rat hippocampus neurons. *Journal of cell science* **109 (Pt 4)**, 787-792 (1996).

64 Helmuth, J. A., Paul, G. & Sbalzarini, I. F. Beyond co-localization: inferring spatial interactions between sub-cellular structures from microscopy images. *BMC Bioinformatics* **11**, 372, doi:10.1186/1471-2105-11-372 (2010).

65 Covill-Cooke, C. L.-D., G.; Birsa, N.; Kittler, J. T. The mitochondrial Rho-GTPase, Miro, is resident at peroxisomes and regulates peroxisomal trafficking and morphology. *BioRxiv*, doi:https://doi.org/10.1101/241208 (2017).

66 Thery, M. Micropatterning as a tool to decipher cell morphogenesis and functions. *Journal of cell science* **123**, 4201-4213, doi:10.1242/jcs.075150 (2010).

67 Lopez-Domenech, G. *et al.* Loss of Dendritic Complexity Precedes Neurodegeneration in a Mouse Model with Disrupted Mitochondrial Distribution in Mature Dendrites. *Cell reports* **17**, 317-327, doi:10.1016/j.celrep.2016.09.004 (2016).

68 Csordas, G., Weaver, D. & Hajnoczky, G. Endoplasmic Reticulum-Mitochondrial Contactology: Structure and Signaling Functions. *Trends in cell biology* **28**, 523-540, doi:10.1016/j.tcb.2018.02.009 (2018).

69 Misko, A., Jiang, S., Wegorzewska, I., Milbrandt, J. & Baloh, R. H. Mitofusin 2 is necessary for transport of axonal mitochondria and interacts with the Miro/Milton complex. *The Journal of neuroscience : the official journal of the Society for Neuroscience* **30**, 4232-4240, doi:10.1523/JNEUROSCI.6248-09.2010 (2010).

70 Norkett, R. *et al.* DISC1-dependent Regulation of Mitochondrial Dynamics Controls the Morphogenesis of Complex Neuronal Dendrites. *The Journal of biological chemistry* **291**, 613-629, doi:10.1074/jbc.M115.699447 (2016).

71 Park, Y. U. *et al.* Disrupted-in-schizophrenia 1 (DISC1) plays essential roles in mitochondria in collaboration with Mitofilin. *Proceedings of the National Academy of Sciences of the United States of America* **107**, 17785-17790, doi:10.1073/pnas.1004361107 (2010).

72 Ivanova, H. *et al.* Inositol 1,4,5-trisphosphate receptor-isoform diversity in cell death and survival. *Biochimica et biophysica acta* **1843**, 2164-2183, doi:10.1016/j.bbamcr.2014.03.007 (2014).

73 Johny, J. P., Plank, M. J. & David, T. Importance of Altered Levels of SERCA, IP3R, and RyR in Vascular Smooth Muscle Cell. *Biophys J* **112**, 265-287, doi:10.1016/j.bpj.2016.11.3206 (2017).

74 Abou-Saleh, H. *et al.* Inositol 1,4,5-trisphosphate (IP3) receptor up-regulation in hypertension is associated with sensitization of Ca2+ release and vascular smooth muscle contractility. *The Journal of biological chemistry* **288**, 32941-32951, doi:10.1074/jbc.M113.496802 (2013).

75 Groigno, L. & Whitaker, M. An anaphase calcium signal controls chromosome disjunction in early sea urchin embryos. *Cell* **92**, 193-204 (1998).

76 Wojcikiewicz, R. J., Pearce, M. M., Sliter, D. A. & Wang, Y. When worlds collide: IP(3) receptors and the ERAD pathway. *Cell Calcium* **46**, 147-153, doi:10.1016/j.ceca.2009.05.002 (2009).

77 Ilacqua, N. *et al.* Protein Localization at Mitochondria-ER Contact Sites in Basal and Stress Conditions. *Front Cell Dev Biol* **5**, 107, doi:10.3389/fcell.2017.00107 (2017).

78 Harner, M. *et al.* The mitochondrial contact site complex, a determinant of mitochondrial architecture. *The EMBO journal* **30**, 4356-4370, doi:10.1038/emboj.2011.379 (2011).

79 Alkhaja, A. K. *et al.* MINOS1 is a conserved component of mitofilin complexes and required for mitochondrial function and cristae organization. *Molecular biology of the cell* **23**, 247-257, doi:10.1091/mbc.E11-09-0774 (2012).

80 Kusumi, A. *et al.* Paradigm shift of the plasma membrane concept from the two-dimensional continuum fluid to the partitioned fluid: high-speed single-molecule tracking

of membrane molecules. *Annu Rev Biophys Biomol Struct* **34**, 351-378, doi:10.1146/annurev.biophys.34.040204.144637 (2005).

81 Sheng, Z. H. Mitochondrial trafficking and anchoring in neurons: New insight and implications. *J Cell Biol* **204**, 1087-1098, doi:10.1083/jcb.201312123 (2014).

82 MacAskill, A. F. & Kittler, J. T. Control of mitochondrial transport and localization in neurons. *Trends in cell biology* **20**, 102-112, doi:10.1016/j.tcb.2009.11.002 (2010).

83 Maeder, C. I., Shen, K. & Hoogenraad, C. C. Axon and dendritic trafficking. *Current opinion in neurobiology* **27C**, 165-170, doi:10.1016/j.conb.2014.03.015 (2014).

84 Schwarz, T. L. Mitochondrial trafficking in neurons. *Cold Spring Harbor perspectives in biology* **5**, doi:10.1101/cshperspect.a011304 (2013).

85 Wideman, J. G. & Munoz-Gomez, S. A. The evolution of ERMIONE in mitochondrial biogenesis and lipid homeostasis: An evolutionary view from comparative cell biology. *Biochimica et biophysica acta* **1861**, 900-912, doi:10.1016/j.bbalip.2016.01.015 (2016).

86 van der Laan, M., Bohnert, M., Wiedemann, N. & Pfanner, N. Role of MINOS in mitochondrial membrane architecture and biogenesis. *Trends in cell biology* **22**, 185-192, doi:10.1016/j.tcb.2012.01.004 (2012).

87 Birsa, N. *et al.* Lysine 27 ubiquitination of the mitochondrial transport protein miro is dependent on serine 65 of the parkin ubiquitin ligase. *The Journal of biological chemistry* **289**, 14569-14582, doi:10.1074/jbc.M114.563031 (2014).

88 Fransson, A., Ruusala, A. & Aspenstrom, P. Atypical Rho GTPases have roles in mitochondrial homeostasis and apoptosis. *The Journal of biological chemistry* **278**, 6495-6502, doi:10.1074/jbc.M208609200 (2003).

89 Chen, H. *et al.* Mitofusins Mfn1 and Mfn2 coordinately regulate mitochondrial fusion and are essential for embryonic development. *J Cell Biol* **160**, 189-200 (2003).

90 Stephen, T. L. *et al.* Miro1 Regulates Activity-Driven Positioning of Mitochondria within Astrocytic Processes Apposed to Synapses to Regulate Intracellular Calcium Signaling. *The Journal of neuroscience : the official journal of the Society for Neuroscience* **35**, 15996-16011, doi:10.1523/JNEUROSCI.2068-15.2015 (2015).

91 Vaccaro, V., Devine, M. J., Higgs, N. F. & Kittler, J. T. Miro1-dependent mitochondrial positioning drives the rescaling of presynaptic Ca2+ signals during homeostatic plasticity. *EMBO reports* **18**, 231-240, doi:10.15252/embr.201642710 (2017).

92 Atkin, T. A., Brandon, N. J. & Kittler, J. T. Disrupted in Schizophrenia 1 forms pathological aggresomes that disrupt its function in intracellular transport. *Hum Mol Genet* **21**, 2017-2028, doi:10.1093/hmg/dds018 (2012).

93 Davenport, E. C. *et al.* Autism and Schizophrenia-Associated CYFIP1 Regulates the Balance of Synaptic Excitation and Inhibition. *Cell reports* **26**, 2037-2051 e2036, doi:10.1016/j.celrep.2019.01.092 (2019).

94 Lowe, A. R. *et al.* Importin-beta modulates the permeability of the nuclear pore complex in a Ran-dependent manner. *Elife* **4**, doi:10.7554/eLife.04052 (2015).

95 Malkusch, S. & Heilemann, M. Extracting quantitative information from single-molecule super-resolution imaging data with LAMA - LocAlization Microscopy Analyzer. *Sci Rep* **6**, 34486, doi:10.1038/srep34486 (2016).

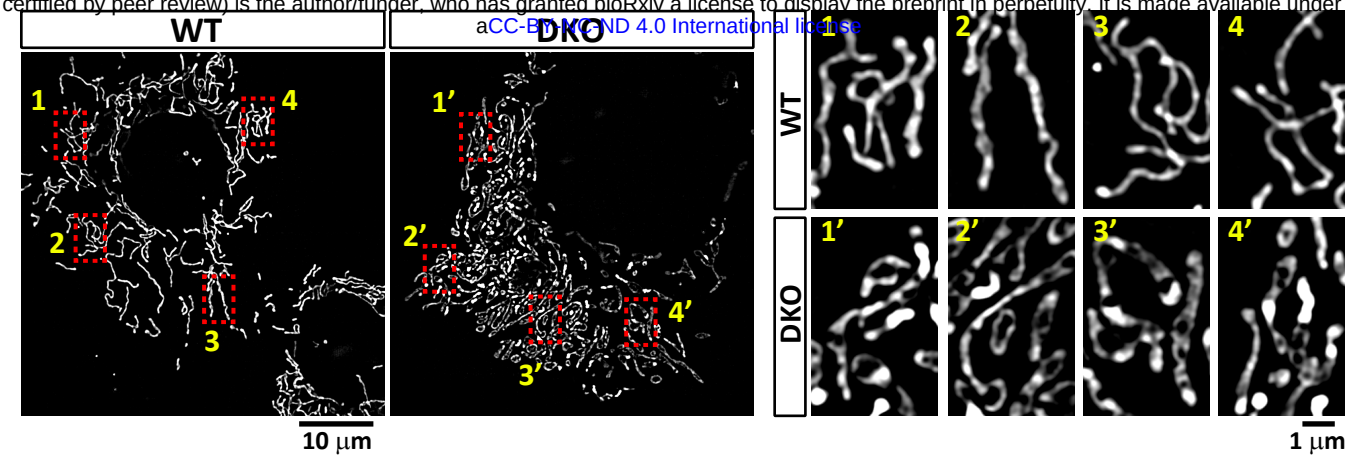

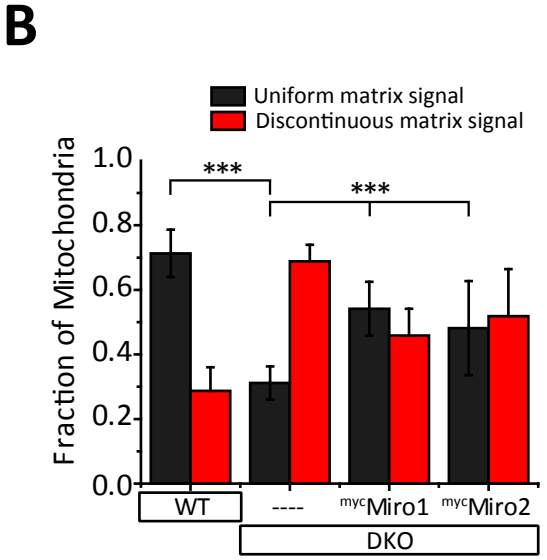

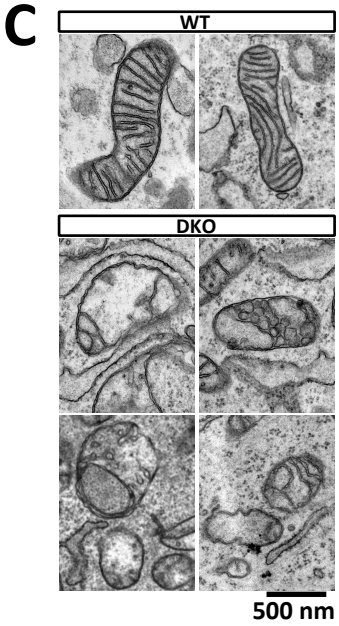

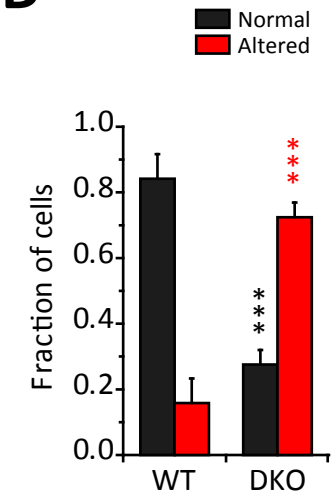

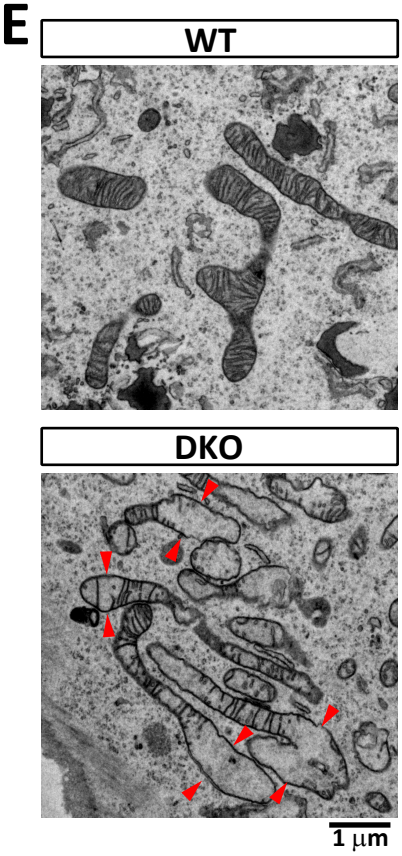

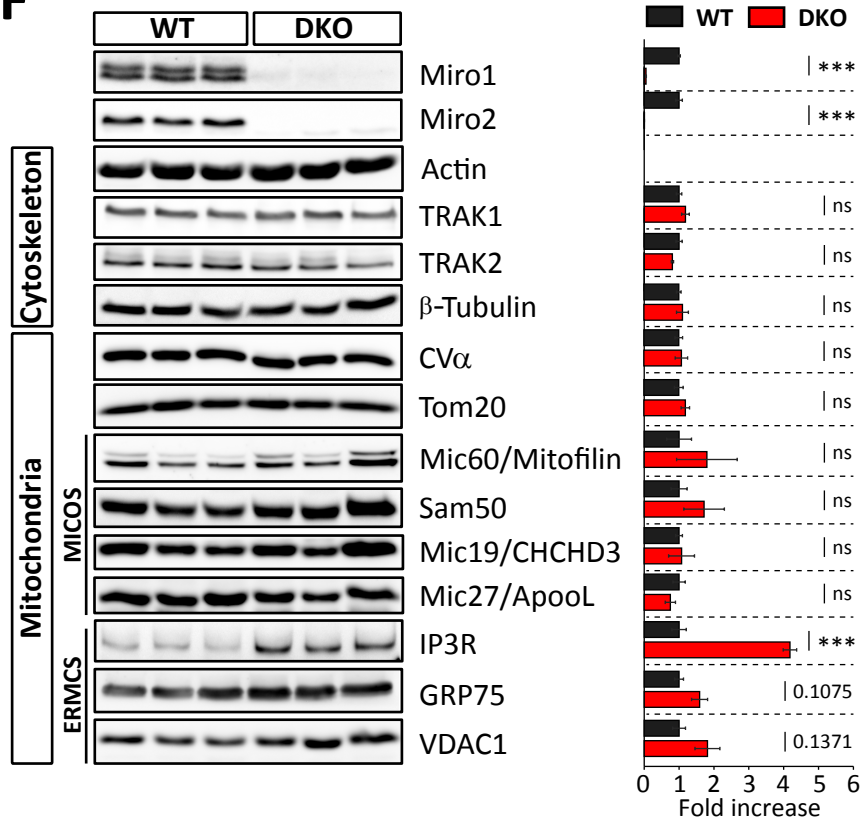

Figure 1

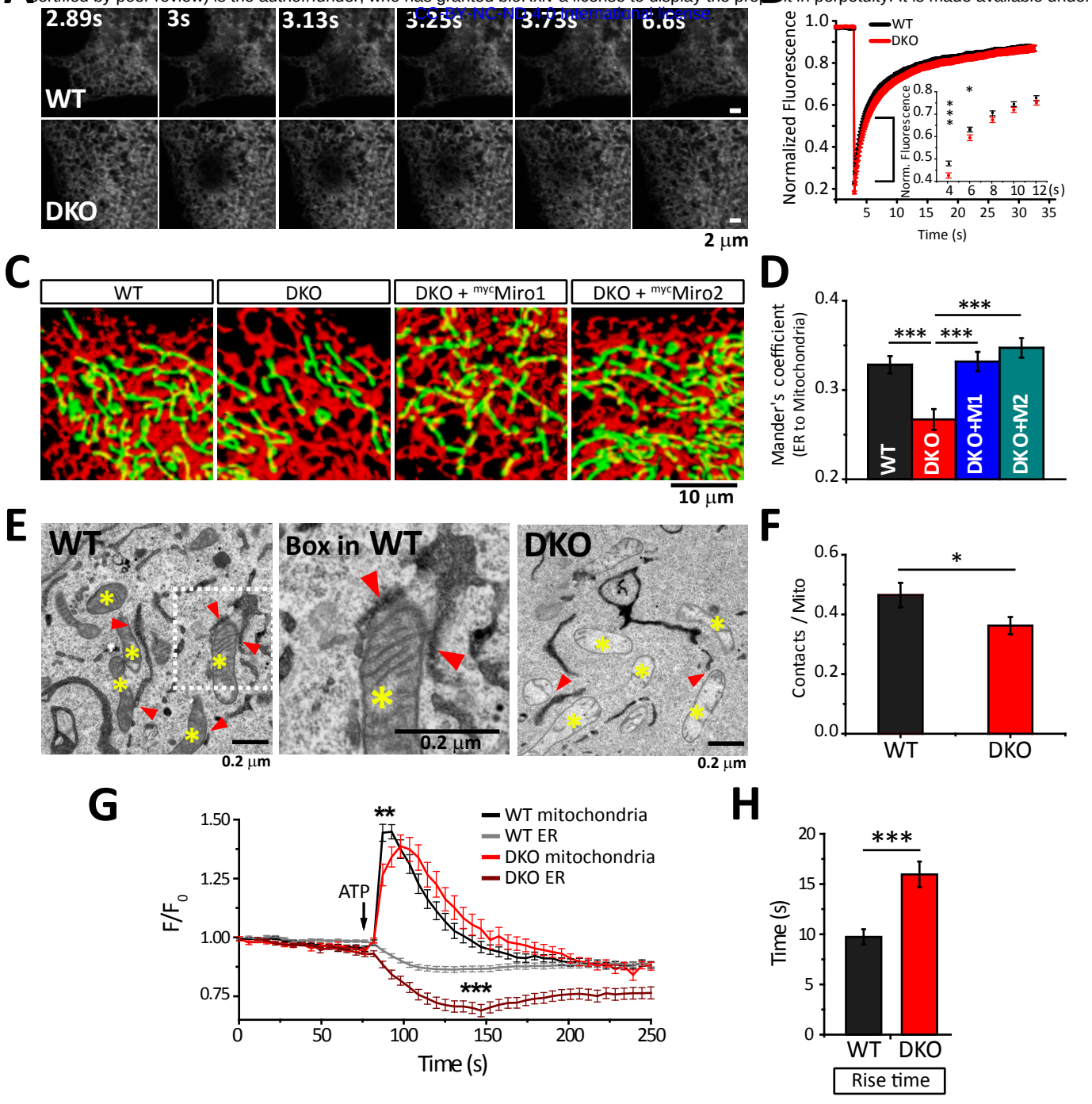

Figure 2

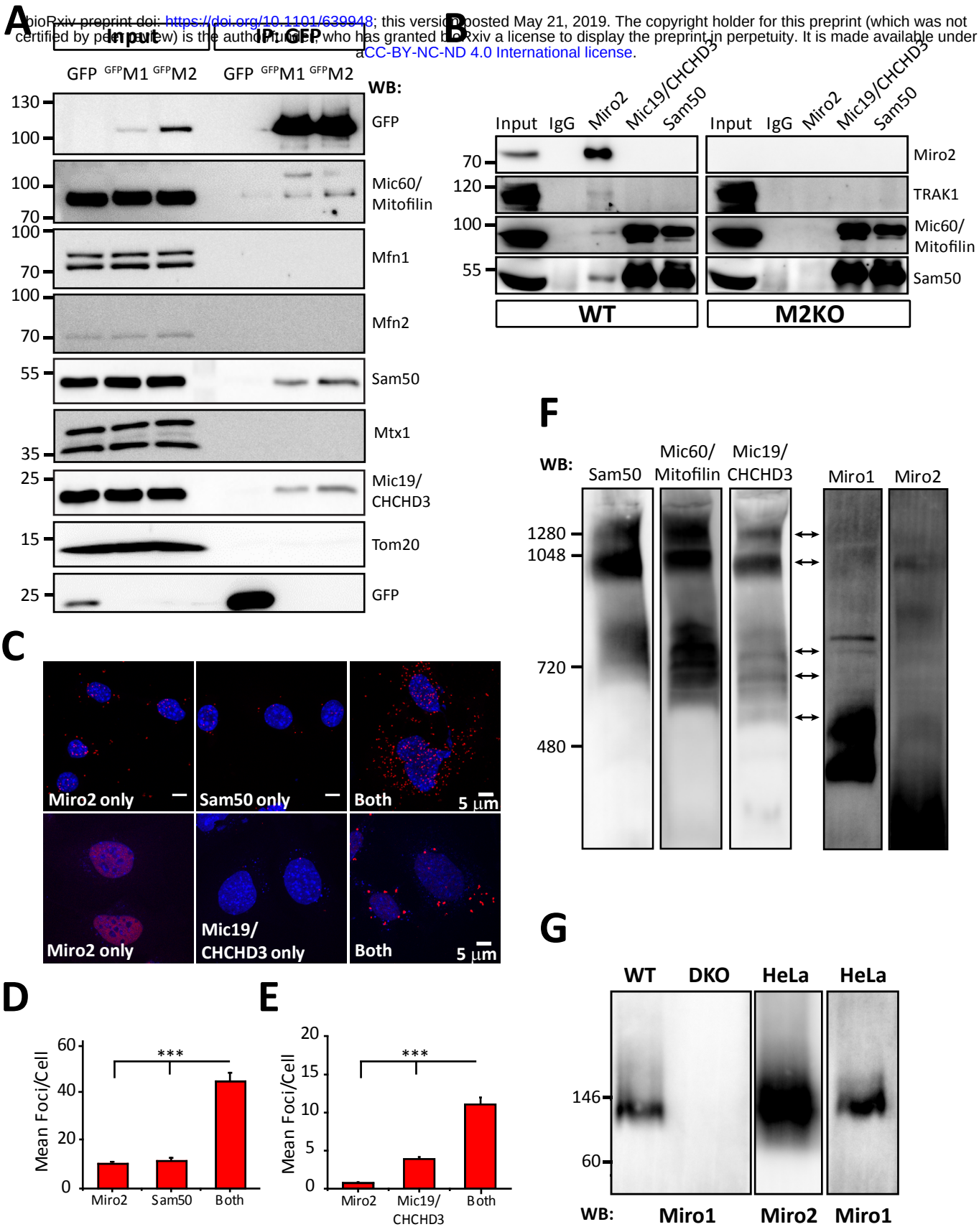

Figure 3

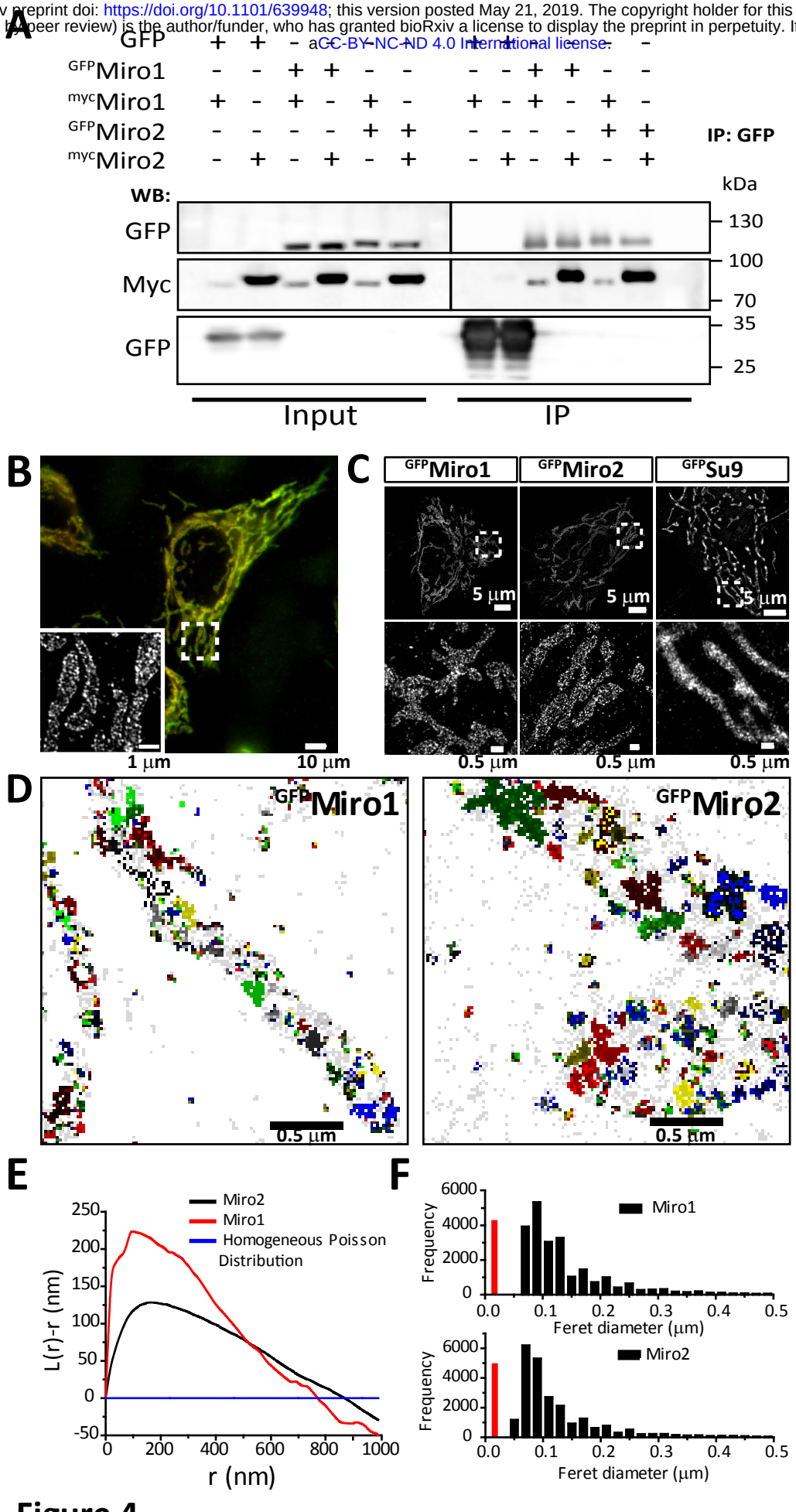

Figure 4

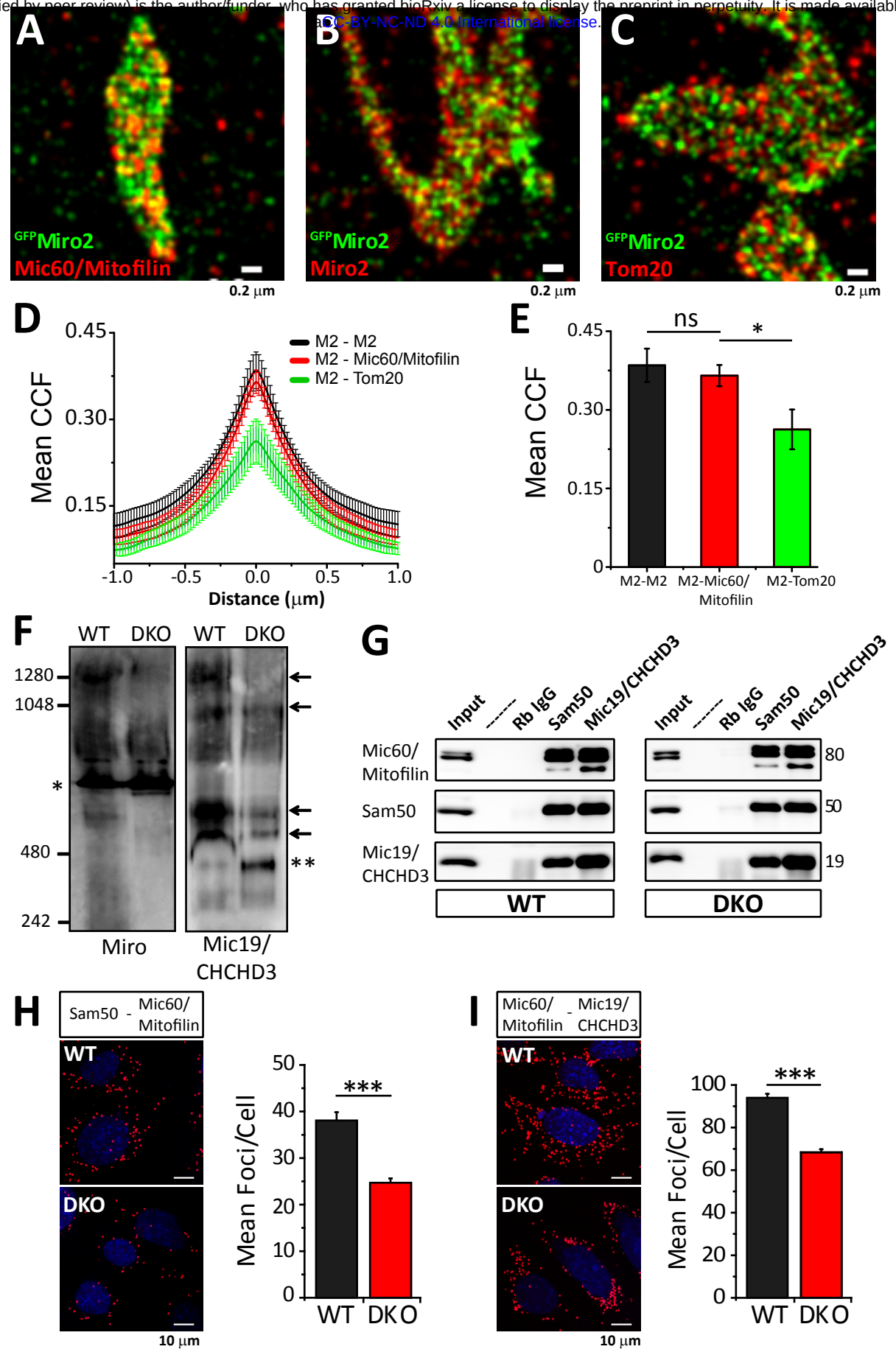

Figure 5

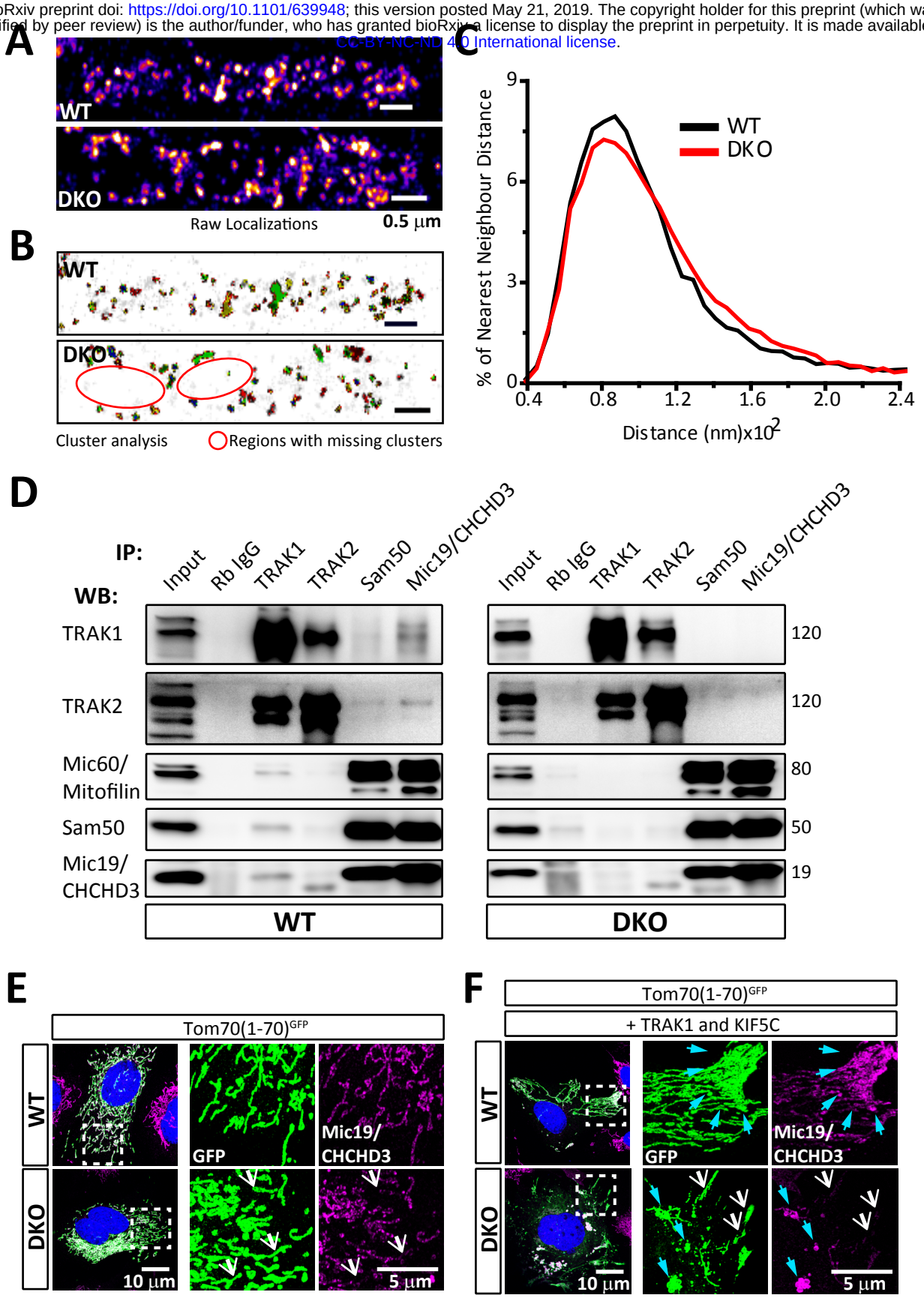

Figure 6

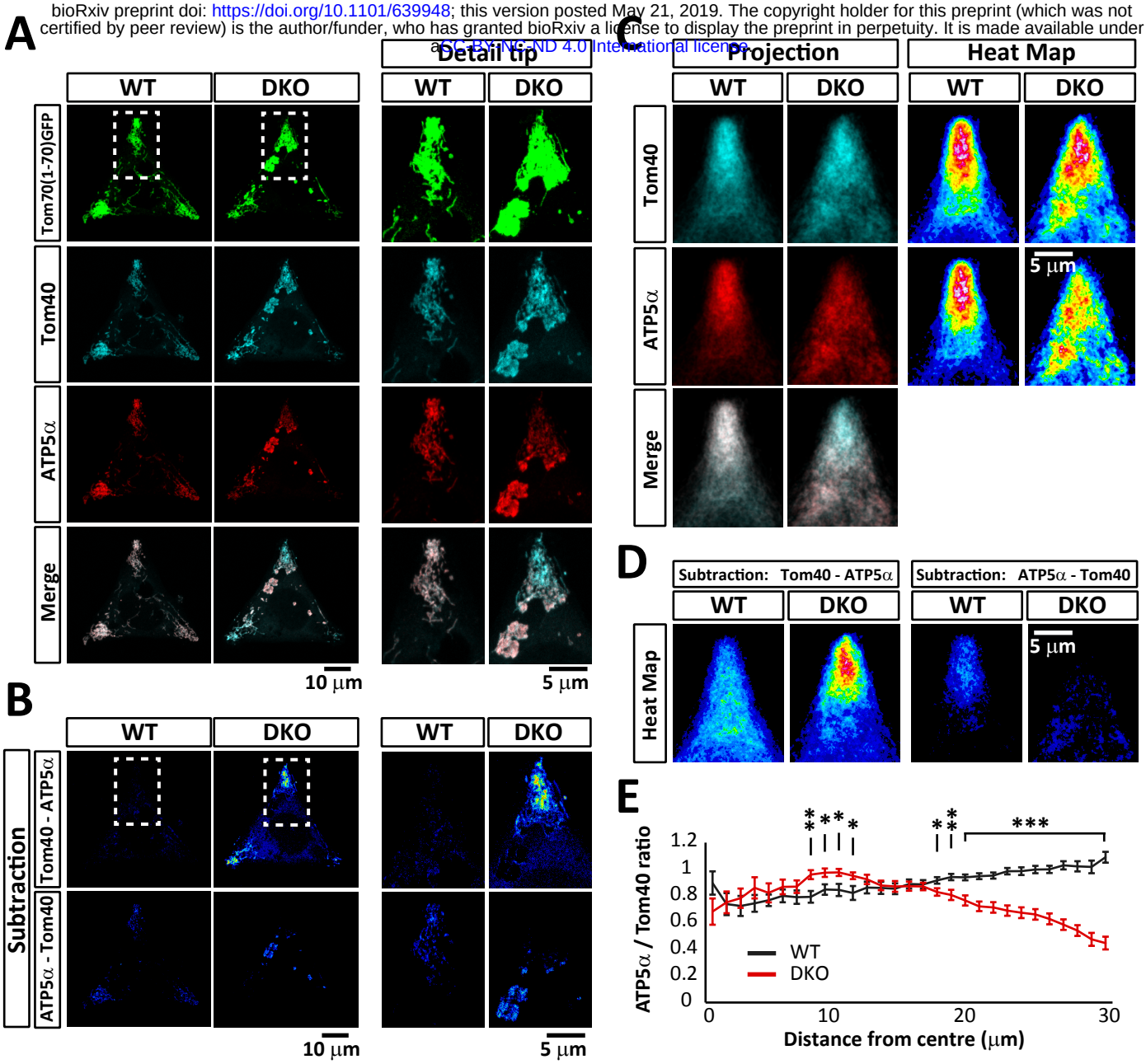

Figure 7